



Formation of highly oxygenated organic molecules from the oxidation of limonene by OH radical: significant contribution of H-abstraction pathway

Hao Luo^{1,2}, Luc Vereecken³, Hongru Shen^{1,2}, Sungah Kang³, Iida Pullinen^{3,a}, Mattias Hallquist⁴, Hendrik Fuchs^{3,5}, Andreas Wahner³, Astrid Kiendler-Scharr^{3,†}, Thomas F. Mentel³, and Defeng Zhao^{1,2,6,7,8}

¹Department of Atmospheric and Oceanic Sciences & Institute of Atmospheric Sciences, Fudan University, Shanghai 200438, China

²National Observations and Research Station for Wetland Ecosystems of the Yangtze Estuary, Fudan University, Shanghai 200438, China

³Institute of Energy and Climate Research, IEK-8: Troposphere, Forschungszentrum Jülich, 52425 Jülich, Germany

⁴Department of Chemistry and Molecular biology, University of Gothenburg, 41258 Gothenburg, Sweden

⁵Fachgruppe Physik, Universität zu Köln, 50932 Cologne, Germany

⁶Shanghai Frontiers Science Center of Atmosphere–Ocean Interaction, Fudan University, Shanghai 200438, China

⁷Institute of Eco-Chongming (IEC), 20 Cuiniao Rd., Chongming, Shanghai 202162, China

⁸CMA-FDU Joint Laboratory of Marine Meteorology, Fudan University, Shanghai 200438, China

^anow at: Department of Applied Physics, University of Eastern Finland, 70210 Kuopio, Finland

[†]deceased, 6 February 2023

Correspondence: Defeng Zhao (dfzhao@fudan.edu.cn) and Thomas F. Mentel (t.mentel@fz-juelich.de)

Received: 29 November 2022 – Discussion started: 9 December 2022

Revised: 23 May 2023 – Accepted: 1 June 2023 – Published: 4 July 2023

Abstract. Highly oxygenated organic molecules (HOMs) play a pivotal role in the formation of secondary organic aerosol (SOA). Therefore, the distribution and yields of HOMs are fundamental to understand their fate and chemical evolution in the atmosphere, and it is conducive to ultimately assess the impact of SOA on air quality and climate change. In this study, gas-phase HOMs formed from the reaction of limonene with OH radicals in photooxidation were investigated with SAPHIR (Simulation of Atmospheric PHotochemistry In a large Reaction chamber), using a time-of-flight chemical ionization mass spectrometer with nitrate reagent ion (NO_3^- -CIMS). A large number of HOMs, including monomers (C_{9-10}) and dimers (C_{17-20}), were detected and classified into various families. Both closed-shell products and open-shell peroxy radicals (RO_2) were identified under low NO (0.06–0.1 ppb) and high NO conditions (17 ppb). C_{10} monomers are the most abundant HOM products and account for over 80 % total HOMs. Closed-shell C_{10} monomers were formed from a two peroxy radical family, $\text{C}_{10}\text{H}_{15}\text{O}_x\cdot$ ($x = 6-15$) and $\text{C}_{10}\text{H}_{17}\text{O}_x\cdot$ ($x = 6-15$), and their respective termination reactions with NO, RO_2 , and HO_2 . While $\text{C}_{10}\text{H}_{17}\text{O}_x\cdot$ is likely formed by OH addition to $\text{C}_{10}\text{H}_{16}$, the dominant initial step of limonene plus OH, $\text{C}_{10}\text{H}_{15}\text{O}_x\cdot$, is likely formed via H abstraction by OH. $\text{C}_{10}\text{H}_{15}\text{O}_x\cdot$ and related products contributed 41 % and 42 % of C_{10} HOMs at low and high NO, demonstrating that the H-abstraction pathways play a significant role in HOM formation in the reaction of limonene plus OH. Combining theoretical kinetic calculations, structure–activity relationships (SARs), data from the literature, and the observed RO_2 intensities, we proposed tentative mechanisms of HOM formation from both pathways. We further estimated the molar yields of HOMs to be $1.97_{-1.06}^{+2.52}$ % and $0.29_{-0.16}^{+0.38}$ % at low and high NO, respectively. Our study highlights

the importance of H abstraction by OH and provides the yield and tentative pathways in the OH oxidation of limonene to simulate the HOM formation and assess the role of HOMs in SOA formation.

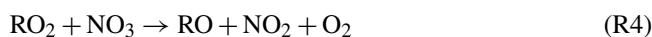
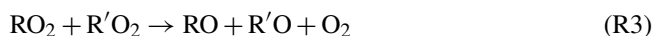
1 Introduction

Biogenic volatile organic compounds (BVOCs) are important precursors of atmospheric secondary organic aerosol particles (SOAs; Griffin et al., 1999; Kanakidou et al., 2005; Hallquist et al., 2009). In the Earth's atmosphere, monoterpenes (C₁₀H₁₆) are abundant BVOCs, with the second-largest emission rate of approximately 150 Tg yr⁻¹ (Guenther et al., 2012). Among them, limonene accounts for 20 % of the total monoterpene emissions, ranking as the fourth largest (Guenther et al., 2012). In addition, as an important ingredient of the essential oil and common volatile chemical product (VCP), limonene is also widely used in house cleaning and personal care products due to its pleasant fragrance and antimicrobial property. Hence, limonene can play an important role in indoor SOA formation and indoor air quality (Waring, 2016; Rossignol et al., 2013; Nazaroff and Weschler, 2004). Although its concentration in the atmosphere is not the most abundant among monoterpenes, limonene has a high potential to form SOAs due to its high SOA yield and the high reactivity provided by the presence of an endocyclic and an exocyclic double bond (Koch et al., 2000; Chen and Hopke, 2010; Gong et al., 2018; Saathoff et al., 2009).

Limonene can undergo gas-phase reactions rapidly with atmospheric oxidants such as the hydroxyl radical (OH) and ozone (O₃) in the daytime and the nitrate radical (NO₃) and O₃ in the nighttime, forming peroxy radicals (RO₂; Lee et al., 2006b; Eddingsaas et al., 2012; Vereecken and Peeters, 2000, 2012; Zhang et al., 2018; Yu et al., 1999). In the reaction of limonene with OH, which is the main atmospheric daytime loss process of limonene, OH addition to one of the olefinic carbon atoms is the dominant channel, although the abstraction of an allylic hydrogen atom also occurs (Rio et al., 2010; Jokinen et al., 2014). Via OH addition, the reaction forms C₁₀H₁₇O₃• as a first-generation RO₂, which, under oxidative conditions, further reacts with RO₂, HO₂, and NO, forming oxidation products including limonaldehyde (C₁₀H₁₆O₂), limonaketone (C₉H₁₄O), limonic acid (C₁₀H₁₆O₃), ketolimononic acid (C₉H₁₄O₄), peroxy-pinonic acid or its isomer (C₁₀H₁₄O₅), nitric acid ester (C₉H₁₃NO₇), some organic acids with low molecular weight (formic acid, acetic acid, butyric acid, and methacrylic), and formaldehyde (HCHO; Pang et al., 2022; Friedman and Farmer, 2018; Romonosky et al., 2015; Jaoui et al., 2006; Lee et al., 2006a; Hakola et al., 1994). Although earlier studies have gained valuable insights into the products and mechanism of the reaction with OH, many products and their formation mechanisms are not well elucidated. For example, highly oxy-

genated organic molecule (HOM) products and their formation mechanism remain elusive.

HOMs were first discovered to be produced in forests and are defined as compounds containing six or more oxygen atoms formed in the gas phase via autoxidation (Bianchi et al., 2019; Ehn et al., 2012; Ehn et al., 2014). Among the myriad of oxygenated products, HOMs were found to be of great importance for the mass of SOA, new particle formation, and particle growth (Jokinen et al., 2014, 2015; Ehn et al., 2014, 2017; Mentel et al., 2015; Molteni et al., 2019; Kirkby et al., 2016; McFiggans et al., 2019; Crouse et al., 2013; Kenseth et al., 2018; Krechmer et al., 2015; Quéléver et al., 2019; Tröstl et al., 2016). Typically, HOMs are generated from the autoxidation of peroxy radicals (RO₂), where a new, more oxygenated RO₂ can be formed after an intramolecular H shift, followed by O₂ addition in the resulting alkyl radical (Bianchi et al., 2019; Vereecken and Nozière, 2020; Crouse et al., 2013; Møller et al., 2019; Vereecken et al., 2007; Ehn et al., 2017; Nozière and Vereecken, 2019; Ehn et al., 2014). Bimolecular termination of the autoxidation chain occurs when an RO₂ intermediate reacts with HO₂, RO₂, and NO to form a series of products (see below), which can be classified as organic hydroperoxide (ROOH; Reaction R1a), alcohol (ROH; Reaction R2), and carbonyl (R = O; Reaction R2), alkoxy radicals (RO; Reactions 3 and 4), or organic nitrates (ON; Reaction R5). The molecular masses of the termination products are $M + 1$, $M - 15$, $M - 17$, and $M + 30$, respectively, for an RO₂ with a molecular mass of M (Mentel et al., 2015; Ehn et al., 2014). Meanwhile, unimolecular termination pathways generally lead to the formation of carbonyls (R = O; Reaction R6). In addition, two RO₂ can also undergo an accretion reaction to form HOM dimers (Reaction R7), as seen in the reactions shown below (Berndt et al., 2018a; Valiev et al., 2019; Y. Zhao et al., 2018). Note that the RO₂ reaction in Reaction R2 is considered for primary and secondary RO₂. For tertiary RO₂s, carbonyls cannot be formed. In addition, the unimolecular isomerization of RO (from Reactions R1b and R3–4) could produce RO₂ in the same RO₂ family.



HOM formation in the OH-initiated oxidation of monoterpenes, such as α -pinene and β -pinene, has been studied in the laboratory (Berndt, 2021; Xu et al., 2019; Berndt et al., 2016; Kirkby et al., 2016; Ehn et al., 2014; Shen et al., 2022) and is assumed to mainly start with the OH addition to the C=C double bond. The alkyl radical adduct can rapidly add O₂ to the radical site to form a peroxy radical (Finlayson-Pitts and Pitts, 2000; Ziemann and Atkinson, 2012). A number of monomer and dimer products from several monoterpenes that followed the reaction with the hydroxyl radical (OH) were observed, such as C₁₀H_{14–18}O_{7–11} and C_{19–20}H_{28–32}O_{10–18} (Berndt et al., 2018a; Shen et al., 2022; Xu et al., 2019). Despite the molecular similarities of the HOM monomers or dimer products from different monoterpenes (Jokinen et al., 2015; Ehn et al., 2012, 2014), the HOM yields are quite different between different monoterpenes in a given oxidation reaction (e.g., with O₃ or OH radical; Jokinen et al., 2015). It follows that the HOM formation mechanisms for other monoterpenes may not necessarily be applicable to limonene. Although HOM formation from limonene by ozonolysis and NO₃ has been reported (Jokinen et al., 2015; Guo et al., 2022; Mayorga et al., 2022), to the best of our knowledge, no studies have systematically reported the HOM distribution in limonene plus OH. In the ozonolysis of limonene, Jokinen et al. (2014) attributed some HOMs (C₁₀H₁₇O_x• (x = 5, 7, 9) (RO₂)) to the reaction of limonene with OH produced in ozonolysis by comparing the mass spectra in the presence or absence of an OH scavenger. The composition and the formation mechanism of HOMs in limonene photooxidation by OH remains unclear. Moreover, although the HOM yield of limonene plus OH was determined, this yield was estimated based on the difference in the HOM yield in the ozonolysis both with and without the OH scavenger (HOM yields are 5.3 % (limonene plus O₃) and 0.93 % (limonene plus OH); Jokinen et al., 2015). It is necessary to confirm the yield with its direct determination in the reaction of limonene plus OH. Interestingly, in our previous study, we found that hydrogen abstraction is important for HOM formation in the reaction of α -pinene plus OH (Shen et al., 2022), where intermediate alkoxy radical oxidation steps aid autoxidation by breaking the six-membered and four-membered rings. As limonene plus OH is known to have a high H-abstraction contribution of ~ 34 % (Rio et al., 2010; Dash and Rajakumar, 2015; Braure et al., 2014), it is interesting to compare these two systems due to the similar but subtly different structures of α -pinene and limonene, with both containing a six-membered ring, whereas limonene does not contain a four-membered ring.

In this study, we investigated HOMs from the photooxidation of limonene with OH at low NO (0.06–0.1 ppb or parts per billion) and high NO (17 ppb) with SAPHIR (Simulation of Atmospheric PHotochemistry In a large Reaction chamber) at Forschungszentrum Jülich. HOMs were classified into monomers and dimers, and the product distribution is reported. The yields of HOMs from limonene with OH were

estimated. The formation mechanism of HOMs in the OH reaction is proposed based on molecular formula of HOMs and quantum chemical calculation, in addition to the structure–activity relationships (SARs) of the RO₂ autoxidation rates. The relative importance of the OH addition to C=C double bond and hydrogen abstraction by OH is discussed. We further investigated the effects of NO_x, which changes the HOM composition via altering the RO₂ fate.

2 Methodology

2.1 Experiment design and setup

The experiments were conducted with SAPHIR at Forschungszentrum Jülich, Germany. Details of the chamber have been described in the previous studies (D. Zhao et al., 2018; Zhao et al., 2015a, b, 2021; Rohrer et al., 2005; Shen et al., 2021; Guo et al., 2022). In brief, SAPHIR is a 270 m³ Teflon chamber equipped with a louvre system to switch between natural sunlight for illumination and dark conditions. In this study, the experiments were conducted in sunlight, with the louvres opened. To avoid possible interference due to the long reaction time, the subsequent discussion focuses on the early stage (15 min) of the experiment. The initial experimental conditions are shown in Table S1 in the Supplement.

Gas- and particle-phase species were characterized by a comprehensive set of instruments, with the details described previously (Zhao et al., 2015b). A proton transfer reaction time-of-flight mass spectrometer (PTR-ToF-MS; Ionicon Analytik GmbH, Austria) was used for measuring volatile organic compounds (VOCs). A NO_x analyzer (Eco Physics; TR480) and a UV photometer O₃ analyzer (Ansyco; model O341M) were used to measure the concentrations of NO₂, NO, and O₃, respectively. A laser-induced fluorescence system (LIF) was used to measure the concentrations of OH, HO₂, and RO₂ (Fuchs et al., 2012). Note that the potential artifact in HO₂ measurements from the concurrent chemical conversion of RO₂ in the instrument that is making use of chemical conversion of HO₂ through the reaction with NO can be avoided in this study through NO used so that no corrections of HO₂ concentration measurements are required. The detection of RO₂ radicals relies on the conversion of RO₂ to HO₂ in their reactions with NO. We applied a correction to the RO₂ concentrations (Fuchs et al., 2011). We would like to note that only a few nitrated RO₂ were observed to not form HO₂ in the reaction with NO. In this study, we do not expect that there was large contribution of nitrate RO₂ to the sum of all RO₂, as seen in photochemistry experiments, as there is no significant fraction of nitrate RO₂ formed. A scanning mobility particle sizer spectrometer (SMPS; TSI Incorporated; DMA 3081/CPC 3785) was used to obtain particle number distributions. Temperature and relative humidity were continuously measured.

Before an experiment was conducted, the chamber was flushed with high-purity synthetic air (purity > 99.9999 % N₂ and O₂). Experiments were conducted at ~ 75 % relative humidity (RH) initially. In low NO conditions, no further NO was added, and the background concentration of NO, which mainly stems from HONO photolysis produced via a photolytic process from a Teflon wall, is 0.06–0.1 ppb (Fig. S1 in the Supplement). OH radicals were generated from the photolysis of HONO in both low and high NO experiments, and the HONO was formed from the Teflon chamber wall via a photolytic process. The details have been described by Rohrer et al. (2005). HO₂ was produced from the reaction of O₂ with RO, which can be formed in the reaction of RO₂ plus NO in photooxidation during the experiments. The concentration of limonene was 7 ppb. The reaction time after the roof opened was 8 h. At high NO conditions, 17 ppb NO was added into the chamber first, and limonene was sequentially added after half an hour. The louvres were opened ~ 40 min after adding limonene. To estimate the impact of ozone oxidation during photooxidation, we calculated the reaction rates of VOC plus OH and VOC plus O₃ in the experiments of this study (Fig. S2). During the first 15 min, VOC plus OH accounted for > 99 % limonene loss in both low and high NO conditions. We would like to note that the low NO does not refer to the case in which the RO₂ loss is dominated by the reaction with HO₂, e.g., in a remote ocean environment. At low NO, the RO₂ loss was estimated to be dominated by its reactions with NO in the early period (within ~ 15 min, RO₂ plus HO₂ contributed ~ 15 % to the RO₂ loss), and in later periods, a significant fraction of the RO₂ loss was also contributed by the reaction of RO₂ with HO₂ (Fig. S3), based on the measured NO_x, RO₂, and HO₂ concentrations and their rate constants for the reactions with RO₂ (Jenkin et al., 1997, 2019). At high NO, the RO₂ fate was by far dominated by the RO₂ plus NO reaction.

2.2 Characterization of HOMs

HOMs were characterized by a chemical ionization time-of-flight mass spectrometer (CIMS; Aerodyne Research Inc., USA) with nitrate (¹⁵NO₃⁻) as the reagent ion, which has a mass resolution of ~ 4000 (m Δm⁻¹). The details of the instrument are described in previous publications (Pullinen et al., 2020; Mentel et al., 2015; Ehn et al., 2014). Briefly, ¹⁵NO₃⁻, which was produced from ¹⁵N nitric acid, was used as the reagent ion to distinguish the complexation with the reagent ion from the NO₃ groups in target molecules. NO₃⁻ CIMS is suitable for detecting oxygenated organic compounds with a high oxygen number. The mass spectra were analyzed by Tofware (version 2.5.7, TOFWERK/Aerodyne Research Inc.) in Igor Pro (version 6.37; WaveMetrics, Inc.). In this study, the mass spectra of HOM products during the first 15 min after the louvres were opened were analyzed because the particle number concentration (< 30 # cm⁻³, where # refers to the particle numbers) remained low in the

initial phase of the reaction. After attributing the molecular formulas of HOMs to different *m/z* (mass-to-charge ratio), their concentrations were calculated using the calibration coefficient of H₂SO₄ (*C* is 2.5 × 10¹⁰ molec. cm⁻³ nc⁻¹), as described before (Zhao et al., 2021; Pullinen et al., 2020), where the charge efficiency of HOMs and H₂SO₄ was assumed to be close to the collision limit (Pullinen et al., 2020; Ehn et al., 2014). The details of the calibration with H₂SO₄ are described in Sect. S1 in the Supplement. The loss of HOMs was corrected by using a wall loss rate of 2.2 × 10⁻³ s⁻¹ in fan-on conditions and ~ 6.0 × 10⁻⁴ s⁻¹ in fan-off conditions, as quantified previously (Guo et al., 2022; D. Zhao et al., 2018), and a dilution loss rate ~ 1 × 10⁻⁶ s⁻¹ (Zhao et al., 2015b). For details, we refer the reader to the aforementioned publications; briefly, the wall loss rate of HOMs in our chamber was estimated as being that of the decay of organic vapor (such as C₁₀H₁₅NO_{9–12} (nitrated compounds) and C₁₀H₁₄O_{8–11} (non-nitrated compounds) in the reaction of limonene with OH in the presence of NO) concentrations in the dark (Guo et al., 2022). Overall, the wall loss correction and dilution correction only affect the HOM yield by ~ 5.8 % and < 1 %, respectively.

2.3 Data analysis

The HOM yield was obtained using the concentration of the HOMs, divided by the concentration of limonene consumed by OH, which is the dominant oxidant of limonene and accounts for over 99 % of the limonene loss rate. HOM yield was calculated over the first 15 min after the opening of the louvres as follows:

$$Y = \frac{[\text{HOM}]}{[\text{VOC}]_r} = \frac{I_{\text{HOM}} \cdot C}{[\text{VOC}]_r}, \quad (1)$$

where [HOM] means the concentrations of total HOMs corrected for wall loss and dilution loss, [VOC]_r is the consumption concentrations of limonene corrected for wall loss and dilution loss, *I*_{HOM} is the total signal intensity of HOMs normalized to the total signal, and *C* is the calibration coefficient of H₂SO₄. The calibration and wall loss and dilution loss correction are described in detail in the Supplement (Sect. S1).

Based on the C₁₀ closed-shell products from unimolecular and bimolecular reactions of the C₁₀ peroxy radical families C₁₀H₁₅O_x• and C₁₀H₁₇O_x•, C₁₀H₁₆O_x can be divided into carbonyls (R = O) and epoxides from C₁₀H₁₇O_x•, in addition to alcohols (ROH) and hydroperoxides (ROOH) from C₁₀H₁₅O_x•. The contribution of C₁₀H₁₇O_x•-related products to C₁₀H₁₆O_x was quantified as follows. For HOM-RO₂, the production rate of alcohols (ROH) can be obtained according to Reaction R2.

$$\frac{d[\text{ROH}]}{dt} = \alpha k_{\text{RO}_2+\text{RO}_2} [\text{RO}_2] [\text{RO}_2]^T \quad (2)$$

The production rate of hydroperoxides (ROOH) can be obtained according to Reaction R1a, which forms ROOH with

a yield β , where β is close to 1 for most RO_2 (Jenkin et al., 2019).

$$\frac{d[\text{ROOH}]}{dt} = k_{\text{RO}_2+\text{HO}_2} [\text{RO}_2] [\text{HO}_2] \beta \quad (3)$$

The production rate of carbonyls ($\text{R}=\text{O}$) can be obtained according to Reactions R2 and R6.

$$\frac{d[\text{R}=\text{O}]}{dt} = (1-\alpha)k_{\text{RO}_2+\text{RO}_2} [\text{RO}_2] [\text{RO}_2]^{\text{T}} + k_{\text{uni}} [\text{RO}_2] \quad (4)$$

By combining Eqs. (2)–(4), one can obtain Eq. (5), as follows:

$$\begin{aligned} \frac{\frac{d[\text{ROH}]}{dt} + \frac{d[\text{ROOH}]}{dt}}{\frac{d[\text{R}=\text{O}]}{dt}} &= \frac{\alpha k_{\text{RO}_2+\text{RO}_2} [\text{RO}_2] [\text{RO}_2]^{\text{T}} + k_{\text{RO}_2+\text{HO}_2} [\text{RO}_2] [\text{HO}_2] \beta}{(1-\alpha)k_{\text{RO}_2+\text{RO}_2} [\text{RO}_2] [\text{RO}_2]^{\text{T}} + k_{\text{uni}} [\text{RO}_2]} \\ &= \frac{\alpha k_{\text{RO}_2+\text{RO}_2} [\text{RO}_2]^{\text{T}} + k_{\text{RO}_2+\text{HO}_2} [\text{HO}_2] \beta}{(1-\alpha)k_{\text{RO}_2+\text{RO}_2} [\text{RO}_2]^{\text{T}} + k_{\text{uni}}}, \end{aligned} \quad (5)$$

where $[\text{RO}_2]^{\text{T}}$ and $[\text{HO}_2]$ are the total concentrations of RO_2 and the concentration of HO_2 in the reaction system, respectively. k_{uni} , $k_{\text{RO}_2+\text{RO}_2}$, and $k_{\text{RO}_2+\text{HO}_2}$ represent the rate coefficient of the unimolecular termination of RO_2 and the bimolecular reactions of RO_2 with RO_2 and HO_2 . α and $1-\alpha$ are the carbonyl yield and the alcohol yield in reactions of RO_2 plus RO_2 , respectively. Wall loss was neglected, due to its minor effects on the concentrations of the products ($\sim 5.8\%$).

For the $\text{C}_{10}\text{H}_{15}\text{O}_x\cdot$ family, Eq. (5) is equivalent to Eq. (6), as follows:

$$\begin{aligned} \frac{\frac{d[\text{ROH}]}{dt} + \frac{d[\text{ROOH}]}{dt}}{\frac{d[\text{R}=\text{O}]}{dt}} &= \frac{\frac{d[\text{C}_{10}\text{H}_{16}\text{O}_x]_{\text{ROH}+\text{ROOH}}}{d[\text{C}_{10}\text{H}_{14}\text{O}_x]}}{\text{C}_{10}\text{H}_{15}\text{O}_x\cdot} \\ &= \frac{d[\text{C}_{10}\text{H}_{16}\text{O}_x] \times (1 - [\text{R}=\text{O}] \%) }{d[\text{C}_{10}\text{H}_{14}\text{O}_x]}. \end{aligned} \quad (6)$$

For the $\text{C}_{10}\text{H}_{17}\text{O}_x\cdot$ family, Eq. (5) is equivalent to Eq. (7), as follows:

$$\begin{aligned} \frac{\frac{d[\text{ROH}]}{dt} + \frac{d[\text{ROOH}]}{dt}}{\frac{d[\text{R}=\text{O}]}{dt}} &= \frac{\frac{d[\text{C}_{10}\text{H}_{18}\text{O}_x]}{d[\text{C}_{10}\text{H}_{16}\text{O}_x]_{\text{R}=\text{O}}}}{\text{C}_{10}\text{H}_{17}\text{O}_x\cdot} \\ &= \frac{d[\text{C}_{10}\text{H}_{18}\text{O}_x]}{d[\text{C}_{10}\text{H}_{16}\text{O}_x] \times [\text{R}=\text{O}] \%}. \end{aligned} \quad (7)$$

As shown in Eq. (2), we assume the same k_{uni} , $k_{\text{RO}_2+\text{RO}_2}$, $k_{\text{RO}_2+\text{HO}_2}$, α , and β for a given $\text{C}_{10}\text{H}_{15}\text{O}_x\cdot$ and $\text{C}_{10}\text{H}_{17}\text{O}_x\cdot$ family. Consequently, the ratios of $\frac{d[\text{ROH}]+d[\text{ROOH}]}{d[\text{R}=\text{O}]}$ for $\text{C}_{10}\text{H}_{15}\text{O}_x\cdot$ and $\text{C}_{10}\text{H}_{17}\text{O}_x\cdot$ are the same. Equation (8) can then be derived from Eqs. (6) and (7) to yield $[\text{R}=\text{O}] \%$, which represents the contribution of the carbonyls produced from $\text{C}_{10}\text{H}_{17}\text{O}_x\cdot$ to $\text{C}_{10}\text{H}_{16}\text{O}_x$.

$$\begin{aligned} \frac{d[\text{C}_{10}\text{H}_{16}\text{O}_x] \times (1 - [\text{R}=\text{O}] \%)}{d[\text{C}_{10}\text{H}_{14}\text{O}_x]} &= \frac{d[\text{C}_{10}\text{H}_{18}\text{O}_x]}{d[\text{C}_{10}\text{H}_{16}\text{O}_x] \times [\text{R}=\text{O}] \%} \end{aligned} \quad (8)$$

Based on this, about 90.1 % and 98.8 % of $\text{C}_{10}\text{H}_{16}\text{O}_x$ were estimated to be carbonyls from $\text{C}_{10}\text{H}_{17}\text{O}_x\cdot$ at low and high NO, respectively. As the HOMs in this study are likely formed via a six-membered carbon ring opening, as discussed below, most HOM- RO_2 are likely primary or secondary RO_2 , as shown in Schemes 1 and 2 and the RO_2 distribution in Fig. S9. For primary and secondary HOM- RO_2 , although the carbonyl yield and alcohol yield does not necessarily equal to 1, they are most likely to be 1, according to Jenkin et al. (2019). With these equations, we can estimate the carbonyl fractions formed via $\text{C}_{10}\text{H}_{17}\text{O}_x\cdot$ under a reasonable assumption. We did a sensitivity analysis to test the influence of varying the k_{uni} , $k_{\text{RO}_2+\text{RO}_2}$, $k_{\text{RO}_2+\text{HO}_2}$, and α using the ranges of these parameters reported in the literature on the fraction of carbonyl in $\text{C}_{10}\text{H}_{16}\text{O}_x$ and on the importance of the H-abstraction channel in HOM formation. When k_{uni} , $k_{\text{RO}_2+\text{RO}_2}$, $k_{\text{RO}_2+\text{HO}_2}$, and α were varied in the range of $(0.01-1) \times 10^{-12}$, $(0.001-1) \times 10^{-10}$, and $(0.5-2) \times 10^{-11} \text{ cm}^3 \text{ molec.}^{-1} \text{ s}^{-1}$, based on the values in the literature (Crouse et al., 2013; Berndt et al., 2018b; Ziemann and Atkinson, 2012), and 0.5, respectively, one can obtain the yield of carbonyl, according to Eqs. (6) and (7), which ranged from 90 %–96 % at low NO and 97 %–100 % at high NO. This indicated that the yields of carbonyl are not sensitive to these assumptions of k and α .

2.4 Theoretical kinetic study of $\text{C}_{10}\text{H}_{15}\text{O}$ alkoxy and $\text{C}_{10}\text{H}_{15}\text{O}_2$ peroxy radicals

The formation mechanism of $\text{C}_{10}\text{H}_{15}\text{O}$ alkoxy and $\text{C}_{10}\text{H}_{15}\text{O}_2$ peroxy radicals were considered in the theoretical kinetic study. The geometries of the intermediates and transition states for the first steps in the mechanism were first optimized using the M06-2X/cc-pVDZ methodology (Zhao and Truhlar, 2008; Dunning, 1989), with an exhaustive characterization of all conformers for each reactant and transition state. All geometries obtained were thus further optimized at the M06-2X-D3/aug-cc-pVTZ level of theory, which includes D3 diffusion corrections (Goerigk et al., 2017; Grimme et al., 2011). Moments of inertia for molecular rotation and wavenumbers for vibration were obtained at the same level of theory, with a vibrational scaling factor of 0.971 (Alecú et al., 2010; Dunning, 1989). The barrier heights were further improved by single-point calculations at the CCSD(T)/aug-cc-pVTZ level of theory (Dunning et al., 2001; Bartlett and Purvis, 1978; all T1 diagnostics ≤ 0.029). The expected uncertainty of the reaction barrier heights at this level of theory is $\pm 0.5 \text{ kcal mol}^{-1}$. All quantum chemical calculations were performed using the Gaussian 16 software suite (Frisch et al., 2016). The quantum chemical data underlying the theoretical kinetic calculations are provided in the Supplement.

The rate coefficients for the individual reactions at the high-pressure limit were then calculated using a multi-conformer transition state theory (MC-TST; Vereecken and

Peeters, 2003), incorporating the data for all conformers obtained as described previously. Tunneling is accounted for by using an asymmetric Eckart barrier correction (Johnston and Heicklen, 1962; Eckart, 1930). Based on earlier work at a similar level of theory in comparison with experimental data on H migration in $\text{RO}_2\cdot$ radicals with no or only one oxygenated functionality (Vereecken and Nozière, 2020; Nozière and Vereecken, 2019) and the available theoretical literature data on ring closure reactions (Vereecken et al., 2021), we estimate the thermal rates to be accurate to a factor 2 to 3.

2.5 SAR-based mechanism development for autoxidation

The kinetics of the chemistry following the ring breaking is expected to be fairly well described based on structure–activity relationships (SARs), and no explicit theoretical kinetic calculations were performed. We employ the same approach for deducing the mechanism as described in our recent work (Shen et al., 2022). Briefly, we only take into account a limited oxidation network by considering all possible reaction channels and select only the dominant channels, based on the rate predicted by SARs. For the rate coefficients for most H migrations in $\text{RO}_2\cdot$ radicals, we base our findings on the SAR by Vereecken and Nozière (2020); this SAR was reported to reproduce scarce experimental data to within a factor of 2, but for multi-functionalized species, such as those studied in this work, the scatter on the data within each SAR category reaches an order of magnitude. For H migrations in cycloperoxides, we additionally rely on the systematic study by Vereecken et al. (2021), who explicitly calculated the rate coefficients for peroxy radicals formed after $\text{RO}_2\cdot$ ring closure reactions. For those reaction classes that are not covered by either SAR, we estimate a rate by extrapolating the reactivity trends in the SARs, albeit with a large uncertainty. For ring closure reactions in unsaturated $\text{RO}_2\cdot$, we employ the SAR by Vereecken et al. (2021), where it is assumed that the presence of another cycloperoxide ring does not influence the rate. In assessing the fate of a $\text{RO}_2\cdot$ radical with one or more $-\text{OOH}$ groups, we account for the possibility of H atom scrambling, as described extensively in the literature (Praske et al., 2019; Møller et al., 2019; Jørgensen et al., 2016; Nozière and Vereecken, 2019; Knap and Jørgensen, 2017). These fast H migrations between the $-\text{OO}\cdot$ and $-\text{OOH}$ groups are typically much faster than other unimolecular channels, leading to a fast equilibration among all accessible OOH -substituted $\text{RO}_2\cdot$ radicals, and the dominant reaction is chosen among those available to the pool of $\text{RO}_2\cdot$ radicals. We refer to Vereecken and Nozière (2020) for a more detailed description of this feature. In the early stages of the oxidation, we also use the recent work by Piletic and Kleindienst (2022). Finally, for alkoxy radical chemistry, we employ the SARs for decomposition and H migration by Novelli et al. (2021) and Vereecken and Peeters (2009, 2010). For hydroperoxyl-substituted alkoxy radicals, we note ex-

PLICITLY that the H migration of the hydroperoxide H atom, forming an alcohol and a RO_2 radical, is typically very fast, $k(298\text{ K}) \geq 10^{10}\text{ s}^{-1}$ (Vereecken and Nozière, 2020), and is often the most likely loss process in later alkoxy stages in the autoxidation chain. This fast H migration supports competitive autoxidation, even under high NO conditions, despite the formation of alkoxy intermediates that threaten to fragment the molecule.

3 Results and discussion

3.1 Overview of HOM spectra

The mass spectra of gas-phase product HOMs formed in the oxidation of limonene by OH at two different NO_x levels are demonstrated in Fig. 1. The HOM products can be classified according their mass-to-charge ratio (m/z) as either monomers (200–400 Th; including C_6 – C_9 monomers and C_{10} monomers at 320–400 Th) or dimers (480–600 Th; C_{17} – C_{20} dimers). We did not observe any trimer products (Fig. S4). The signal intensity of the monomers is higher than dimers at both low and high NO (Figs. 1 and 2), where monomers accounted for over 80 % of total HOMs. Both the signal intensity and the fraction of the observed dimers at high NO were much lower than that at low NO (Figs. 1 and 2). In the following (Sect. 3.2), we discuss the product distribution and formation mechanism of monomers and dimers in detail.

3.2 Identification and formation mechanism of HOMs

3.2.1 Overview of HOM monomers

Closed-shell HOM monomers are characterized by the repeating pattern of molecular formulas with an increasing number of oxygen atoms in the mass spectrum. The repeating pattern in the mass spectrum at every 16 Th forms a series of HOM monomer families, such as $\text{C}_6\text{H}_{8/10}\text{O}_x$, $\text{C}_6\text{H}_{9/11}\text{NO}_x$, $\text{C}_7\text{H}_{8/10/12}\text{O}_x$, $\text{C}_7\text{H}_{9/11}\text{NO}_x$, $\text{C}_8\text{H}_{10/12/14}\text{O}_x$, $\text{C}_8\text{H}_{11/13}\text{NO}_x$, $\text{C}_9\text{H}_{12/14/16}\text{O}_x$, $\text{C}_9\text{H}_{13/15}\text{NO}_x$, $\text{C}_{10}\text{H}_{14/16/18}\text{O}_x$, and $\text{C}_{10}\text{H}_{15/17}\text{NO}_x$ (Fig. S5). It is worth noting that some open-shell radicals, such as $\text{C}_{10}\text{H}_{15}\text{O}_x\cdot$ ($x = 6$ – 15) and $\text{C}_{10}\text{H}_{17}\text{O}_x\cdot$ ($x = 6$ – 15), were also observed; these are a significant fraction of HOM monomers and will be discussed in detail in Sect. 3.2.2. These open-shell molecules were likely RO_2 radicals, as we are not able to detect the very short-lived alkoxy radicals (RO) and alkyl radicals (R). The closed-shell products ($\text{C}_{\leq 10}\text{H}_y\text{O}_x$ and $\text{C}_{\leq 10}\text{H}_y\text{NO}_x$) will be discussed in the following from the perspective of RO_2 chemistry (i.e., as termination products of RO_2). It should be noted that each molecular mass can represent several isomers and that there may be more than one pathway to form a given product; our experiments do not allow us to discriminate these, and an in-depth discussion is beyond the scope of this work.

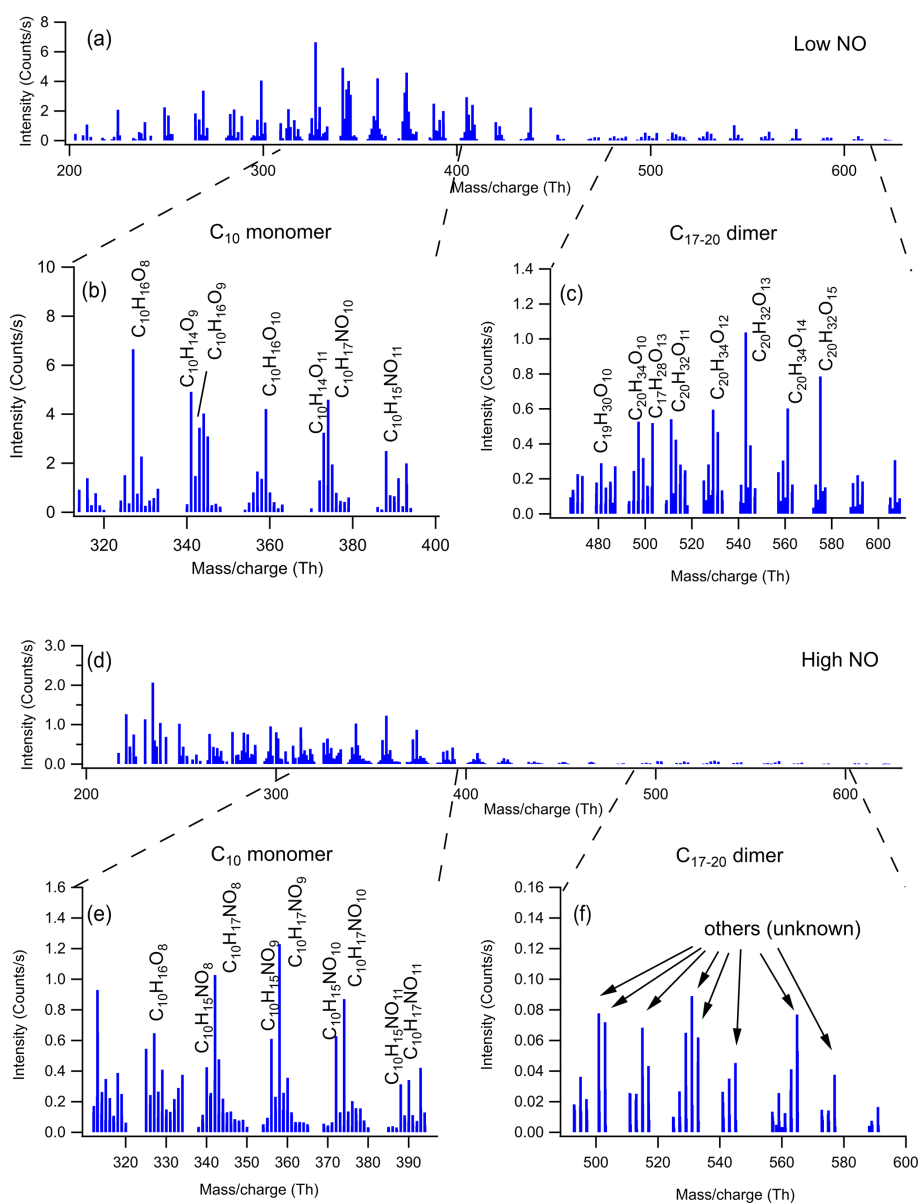


Figure 1. Mass spectrum of the HOMs formed in the oxidation of limonene by OH in (a) low and (d) high NO conditions. The mass spectra were obtained within 15 min after opening the louvres and were averaged over 15 min. (b, c, e, f) The expanded mass spectra are presented, where major peaks are labeled with their molecular formulas.

HOM monomers were classified into C_{10} and C_{6-9} monomers according to the number of carbon atoms. The abundance of C_{6-9} monomers ($\sim 27.0\%$ combined) was lower than the C_{10} compounds ($\sim 46.4\%$) at low NO. In addition to C_{10} and C_{6-9} monomers, other monomers accounted for $\sim 18.9\%$ of all monomers, and unspecified monomers accounted for $\sim 7.7\%$. As shown in Fig. S5, C_{6-10} monomers contain either no or one nitrogen atoms, and a higher fraction of organic nitrates was observed in high NO conditions (nitrate HOMs are 31% at low NO and 41% at high NO). This is as expected, given that the fraction of RO_2 terminated by NO forming organic nitrate was higher at high

NO. Higher fractions of organic nitrate have also been observed by the previous studies in the photooxidation of other monoterpenes at high NO (Pullinen et al., 2020; Shen et al., 2022).

3.2.2 C_{10} monomer product distribution

At low and high NO conditions, C_{10} compounds ($C_{10}H_{14}O_x$, $C_{10}H_{15}NO_x$, $C_{10}H_{16}O_x$, $C_{10}H_{17}NO_x$, and $C_{10}H_{18}O_x$) were the abundant monomers, with a fractional contribution of $\sim 27\% \sim 41\%$ (see Fig. 3). In this study, we observed two major RO_2 radical families, $C_{10}H_{15}O_x\cdot$ ($x = 6-15$) and

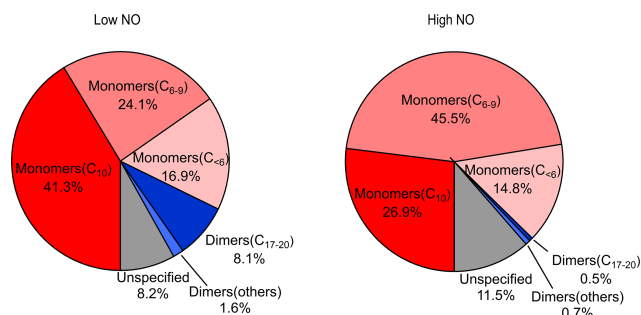


Figure 2. HOM product distribution, including monomers (C_{10} , C_{6-9} , $C_{<6}$), dimers (C_{17-20} ; other), and unspecified species in low and high NO conditions during the first 15 min of the experiments.

$C_{10}H_{17}O_x\cdot$ ($x = 6-15$), and their corresponding termination products, $C_{10}H_{14}O_{x-1}$, $C_{10}H_{16}O_{x-1}$, $C_{10}H_{16}O_x$, and $C_{10}H_{15}NO_{x+1}$ and $C_{10}H_{16}O_{x-1}$, $C_{10}H_{18}O_{x-1}$, $C_{10}H_{18}O_x$, and $C_{10}H_{17}NO_{x+1}$, respectively, which contained carbonyl, hydroxyl, hydroperoxyl, and nitrate, respectively (see Figs. 3 and S5; Tables S2, S3, S6, and S7). $C_{10}H_{14}O_x$ and $C_{10}H_{16}O_x$ were likely carbonyl compounds formed via the unimolecular termination of $C_{10}H_{15}O_x\cdot$ and $C_{10}H_{17}O_x\cdot$, respectively. Overall, at high NO, organic nitrates were the most abundant among all classes of HOM monomers, and their relative proportion was much higher than at low NO (Fig. 3). Under low NO conditions, the $C_{10}H_{14}O_x$ and $C_{10}H_{16}O_x$ family are the two most abundant families among C_{10} monomers. This is similar to the C_{10} monomer products from the photooxidation of α -pinene by OH the radical (Shen et al., 2022).

3.2.3 Monomers with $C_{<10}$ monomers and dimers

A number of monomers with a carbon number less than 10 ($C_{<10}$) was observed in this study. The monomers ($C_{<10}$) account for about 24.1%–45.5% of the total monomers. The two radicals $C_7H_9O_x\cdot$ and $C_7H_{11}O_x\cdot$ were likely produced from $C_{10}H_{15}O_x\cdot$ radicals and $C_{10}H_{17}O_x\cdot$ radicals, respectively (see below). The ratios of the total termination products from $C_7H_9O_x\cdot$ to those from $C_7H_{11}O_x\cdot$ are 0.7 at both low and high NO, which is generally consistent with the ratio of $C_{10}H_{15}O_x\cdot$ radicals and $C_{10}H_{17}O_x\cdot$ radicals for C_{10} -related products. This suggests that the chemistry related to $C_{10}H_{15}O_x\cdot$ radicals plays a significant role in the formation of $C_{<10}$ monomers. Although the concentrations of monomers ($C_{<10}$) are smaller than those of C_{10} monomers, they may also contribute to the formation of dimers, which further condense onto particles.

We observed a number of dimer families, including $C_{20}H_{30}O_x$ ($x = 10, 12-18$), $C_{20}H_{32}O_x$ ($x = 9-18$), $C_{20}H_{34}O_x$ ($x = 10-17$), $C_{19}H_{32}O_x$ ($x = 10-15$), $C_{19}H_{31}NO_x$ ($x = 11-18$), $C_{19}H_{30}O_x$ ($x = 10-17$), $C_{18}H_{30}O_x$ ($x = 10-14$), $C_{19}H_{28}O_x$ ($x = 11-15$), $C_{17}H_{26}O_x$ ($x = 11-15$), and $C_{17}H_{24}O_x$ ($x = 12-17$) in low NO

conditions and $C_{20}H_{30}O_x$ ($x = 12-16$), $C_{20}H_{32}O_x$ ($x = 11-18$), $C_{20}H_{34}O_x$ ($x = 10-15$), $C_{19}H_{28}O_x$ ($x = 11-17$), and $C_{17}H_{26}O_x$ ($x = 12-15$) in high NO conditions (see Tables S4 and S5). Compared to the monomers, the peak intensity of dimers at both low and high NO conditions is much lower (Figs. S7 and S8). Furthermore, the peak intensity of dimers in low NO conditions is higher than that in high NO conditions. This inhibitory effect of NO_x in dimer formation is consistent with the phenomenon described in previous studies (Pullinen et al., 2020; Yan et al., 2016; Shen et al., 2022). In the following discussion, we will focus on C_{10} monomers. However, more information on $C_{<10}$ monomers and dimers can be found in Sect. S2.

3.3 Formation pathways of HOM monomers

In this section, we discuss the potential formation pathways for C_{10} monomers. These pathways are tentative only and are based on the current knowledge of autoxidation, as represented in various SARs, where we examine only those paths estimated as being the fastest. Our observations do not distinguish between different isomers, and we cannot validate the reaction scheme. We also observed HOMs with only 7, 8, or 9 carbon atoms, and their possible formation pathways, which involve a fragmentation step in an intermediate alkoxy radical, are inspected in the Supplement (see Schemes S1 and S2).

3.3.1 HOMs from OH addition

The $C_{10}H_{17}O_x\cdot$ radicals are formed from the OH addition reaction of limonene and subsequent autoxidation (see Table S3). Scheme 1 shows the possible oxidation routes for the OH addition to both double bonds, considering the particular channels leading to tertiary alkyl radicals and depicting the most likely reactions, as estimated based on theoretical work and SARs (Peeters et al., 1999; Vereecken et al., 2007; Jenkin et al., 2018). The $C_{10}H_{17}O_3\cdot$ RO₂ radical formed after O₂ addition to the OH adducts has access to a wide range of reactions, but in most cases, the six-membered ring is retained in the first RO₂ steps, leading to slow autoxidation steps (Vereecken et al., 2021). This allows the reaction with NO to become important, whereafter the decomposition of a β -OH or β -OOH alkoxy radical leads to carbonyl formation and thus chain termination. This analysis suggests that HOM formation after OH addition either proceeds through less favorable pathways or involves secondary chemistry. The complete explicit mechanism is highly branched and complex, and missing pathways in Scheme 1 could together contribute to sizable HOM formation. Furthermore, the rate estimates are tentative, with uncertainties that are an order of magnitude or more, so we cannot exclude that primary HOM formation is possible and important. The primary products predicted in Scheme 1 (or formed through similar termination reactions in other channels) can react again with OH, initi-

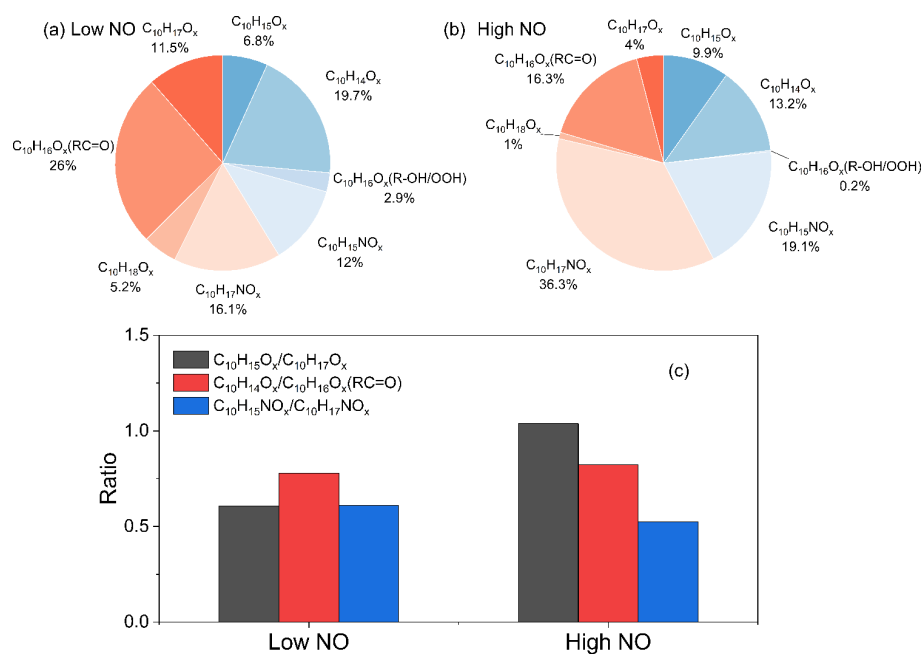


Figure 3. Product distribution within C₁₀ monomers at (a) low and (b) high NO and (c) the ratio of C₁₀H₁₅O_x• to C₁₀H₁₇O_x• and of their termination products. As in Fig. 2, the data of the first 15 min of the experiments were used.

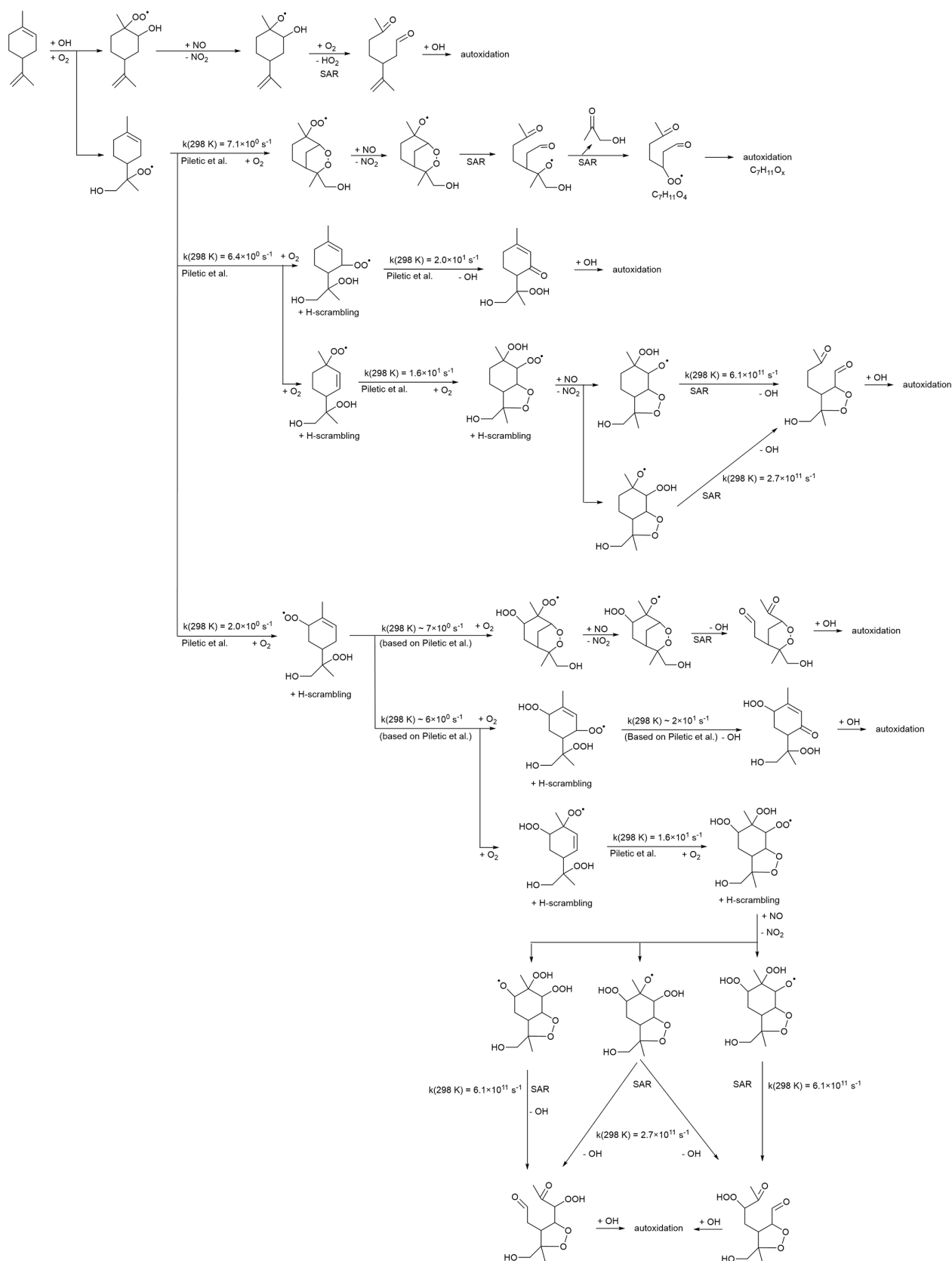
ating secondary autoxidation. Most of these products have the six-membered ring broken and should be more amenable to further autoxidation steps and thus readily yield HOMs. However, this extra bimolecular OH reaction takes time and can delay the formation of HOMs. An analysis of the secondary chemistry is beyond the scope of this work, and at this time, we do not propose a reaction scheme that covers the full range of C₁₀H₁₇O_x• radicals and the related products observed.

In our previous study, the average bimolecular RO₂ loss rate was estimated at $\sim 0.02 \text{ s}^{-1}$ (low NO) and $\sim 3.5 \text{ s}^{-1}$ (high NO; D. Zhao et al., 2018). In both cases, RO₂ loss is due predominantly to the reaction with NO (see Fig. S3), which leads to the organic nitrate termination products, as illustrated in Fig. 3. Even at low NO with ~ 0.2 ppb, organic nitrates contribute a large portion of HOMs (33%). The relevant termination products from C₁₀H₁₇O_x• ($x = 8\text{--}13$) in reactions with HO₂ and RO₂ are identified as C₁₀H₁₈O_x, C₁₀H₁₈O_{x-1}, and C₁₀H₁₆O_{x-1}. However, C₁₀H₁₈O_x accounted for only 5.2% and 1% in C₁₀ monomers at low and high NO, respectively, as in high NO conditions these loss processes are overwhelmed by the RO₂ plus NO reaction.

3.3.2 HOMs from H abstraction by OH

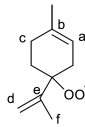
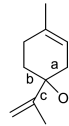
The observed C₁₀H₁₅O_x• radicals mainly originate from an H-abstraction reaction by OH, removing one of the limonene H atoms. In principle, C₁₀H₁₅O_x• peroxy radicals might also form through the secondary chemistry of first-generation C₁₀ oxidation products of the limonene plus OH reaction. The

limonaldehyde (C₁₀H₁₆O₂) is the most abundant (99%) first-generation C₁₀ product reported in limonene plus OH reaction (Hakola et al., 1994; Larsen et al., 2001), which can form C₁₀H₁₅O₄• and the C₁₀H₁₅O_x• family by further autoxidation through H abstraction and subsequent O₂ addition. Therefore, we take into account limonaldehyde that is the most competitive candidate. For the early stages of our experiments (first 15 min), however, we find that secondary chemistry is not important (Sect. S2 and Fig. S9). An example pathway for C₁₀H₁₅O_x• RO₂ radical formation is shown in Scheme 2, based on the most facile H-abstraction channel from limonene. Direct autoxidation of the nascent RO₂ is slow, $k = \sim 10^{-2} \text{ s}^{-1}$, and formation of an alkoxy radical is to be expected immediately or after very few autoxidation steps, especially in high NO conditions. Once the ring structure is broken, fast autoxidation steps are accessible. All RO₂ intermediates have competing reactions (not shown) under current conditions with HO₂ (forming hydroperoxides) and NO (forming alkoxy radicals and nitrates). The alkoxy radicals formed thus can fragment, or continue autoxidation after ring breaking or fast migration of a hydroperoxide H atom, forming a wider variety of HOMs. The nascent peroxy radical formed after the H abstraction of the allylic tertiary H atom in limonene is not amenable to efficient autoxidation and HOM formation, due to the geometric constraints in the ring. Theoretical kinetic calculations (see Table 1) show that the fastest autoxidation steps occur at rates of $\sim 2 \times 10^{-2} \text{ s}^{-1}$ (i.e., of a similar magnitude to the RO₂ loss with NO in the low NO experiments but negligible against the RO₂ plus NO rate at high NO). Our rate predic-



Scheme 1. Example reaction scheme for C₁₀H₁₇O_x•RO₂ formation after OH addition in limonene, based on the most likely reactions predicted in theoretical work and SAR predictions. All RO₂ intermediates have competing reactions (not shown) under the current conditions with HO₂ (forming hydroperoxides) and NO (forming alkoxy and nitrates).

Table 1. H migration, ring closure, and C–C bond scission reactions in RO₂• and RO• radicals formed from limonene H abstraction, listing barrier heights E_b (kcal mol⁻¹), rate coefficient k at 298 K (s⁻¹), and parameters for a Kooij equation fit $k(T) = A \times T^n \times \exp(-E_a/T)$ for the temperature range 200–450 K, calculated using the CCSD(T)//M06-2X-D3 level of theory.

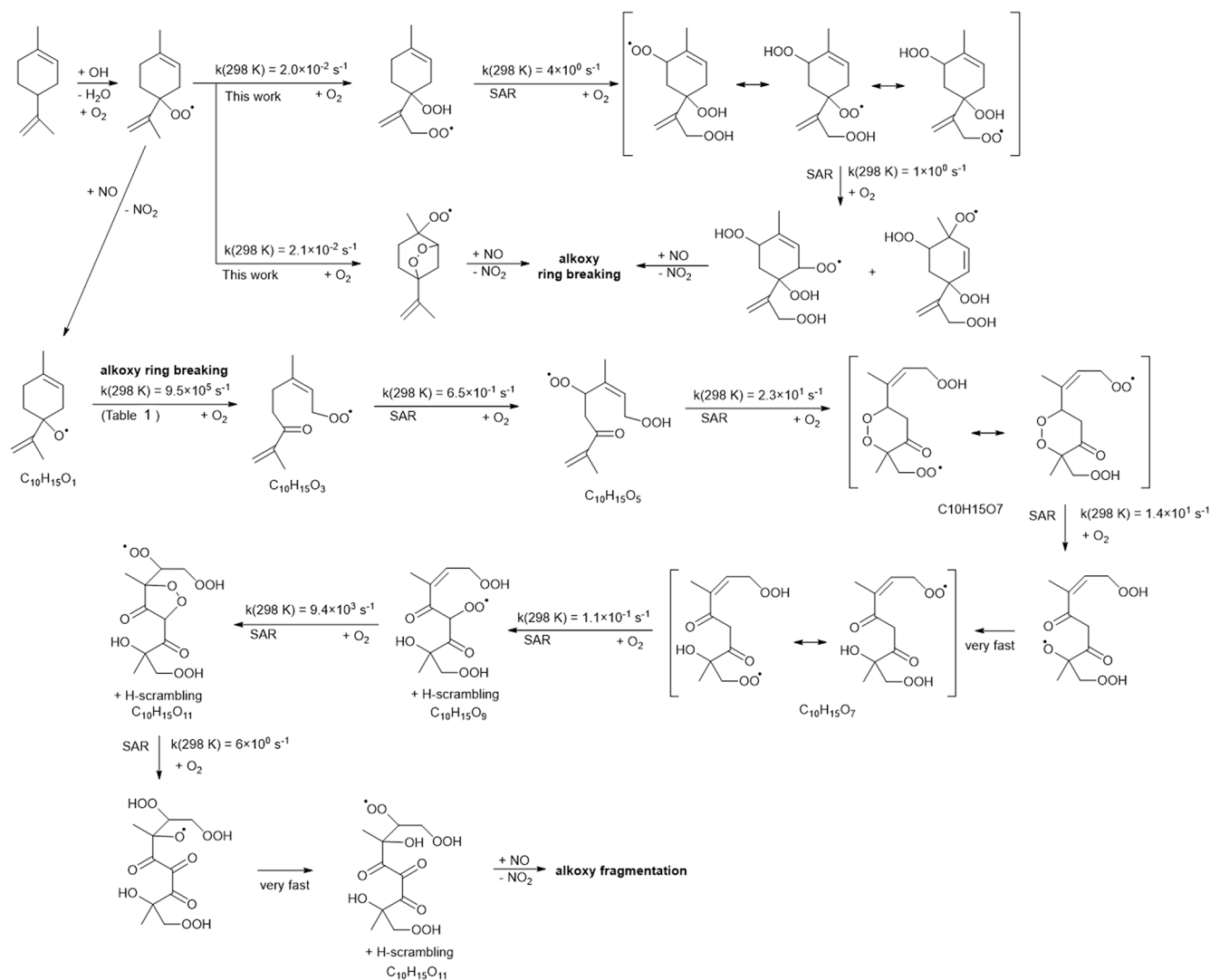
| RO ₂ • | Reaction type | E_b | k (298 K) | A/s^{-1} | n | E_a/K |
|---|-----------------------|-------|-----------------------|------------------------|-------|---------|
|  | Five-ring closure (a) | 19.0 | 2.1×10^{-2} | $5.40 \times 10^{+7}$ | 1.40 | 8840 |
| | Six-ring closure (b) | 20.2 | 1.8×10^{-3} | $6.35 \times 10^{+7}$ | 1.27 | 9390 |
| | Allyl 1,5 H shift (c) | 24.4 | 1.2×10^{-3} | 6.45×10^{-91} | 32.94 | -3977 |
| | Four-ring closure (d) | 26.9 | 2.4×10^{-8} | $2.50 \times 10^{+3}$ | 2.79 | 12 292 |
| | Five-ring closure (e) | 29.8 | 2.3×10^{-10} | $1.04 \times 10^{+3}$ | 2.83 | 13 489 |
| | Allyl 1,5 H shift (f) | 22.5 | 2.0×10^{-2} | 8.68×10^{-81} | 29.51 | -3667 |
| Other H migrations lead to high ring strain and are not competitive | | | | | | |
|  | Ring opening (a) | 9.4 | 9.5×10^5 | $7.60 \times 10^{+8}$ | 1.42 | 4409 |
| | Ring opening (b) | 10.5 | 1.6×10^5 | $1.01 \times 10^{+9}$ | 1.39 | 4972 |
| | Fragmentation (c) | 17.4 | 3.4×10^0 | $2.49 \times 10^{+9}$ | 1.48 | 8602 |
| H migrations or ring closure lead to high ring strain and are not competitive | | | | | | |

tions agree with the recent theoretical study by Piletic and Kleindienst (2022). Further autoxidation steps with the ring structure intact are expected to be unfavorable, as in the case with autoxidation initiated through other H-abstraction sites (Vereecken et al., 2021; Piletic and Kleindienst, 2022). The reaction of the primary RO₂ with NO, however, leads to an alkoxy radical that is most likely to break the six-membered ring, with a total rate coefficient exceeding $\sim 10^6$ s⁻¹ (see Table 1). This alkoxy-peroxy autoxidation step thus removes the geometric constraint, and fast autoxidation reactions become accessible, with rates enhanced by the presence of the double bonds (Vereecken and Nozière, 2020; Møller et al., 2019). Though further alkoxy-peroxy steps are not necessary for HOM formation from limonene, subsequent autoxidation steps will compete against bimolecular reactions with NO, suggesting that more alkoxy-peroxy steps may occur, even when the unimolecular lifetime of these later non-cyclic RO₂ radicals is typically shorter than that of the early-stage cyclic RO₂. Some of these alkoxy intermediates will preferentially break the carbon backbone, leading to fragmentation, while other alkoxy radicals will proceed by H migration and continue the autoxidation chain. In the latter case, autoxidation then no longer follows the systematic series of adding two O atoms per autoxidation step, and the C₁₀H₁₅O_{*x*}• formation mechanism can proceed with both even-numbered and odd-numbered oxygen numbers *x*. At high NO concentrations, formation of alkoxy radicals becomes more likely, and thus fragmentation can become more prominent, reducing the yield of C₁₀H₁₅O_{*x*}•-related HOMs. This is in agreement with the current observations, where more fragment C_{<10} monomers (47.2 % in total monomers) are observed at high NO than at low NO (27.0 %). Further autoxidation of the fragments is also possible, leading to C_{<10} monomers and dimer formation, as discussed in the Supplement. The need for a ring-breaking alkoxy-peroxy step in the proposed HOM formation mechanism does suggest that the highest yields of

limonene HOM formation may occur at slightly higher NO concentrations than for non-cyclic VOCs, which autoxidize, even without alkoxy steps.

3.3.3 Relative contribution of OH addition versus OH H abstraction

As C₁₀H₁₅O_{*x*}• (*x* = 6–15) is formed via the OH H-abstraction pathway and C₁₀H₁₇O_{*x*}• is formed via OH addition, we can compare the relative importance of these two pathways via the ratios of C₁₀H₁₅O_{*x*}• to C₁₀H₁₇O_{*x*}• radicals and their termination products. At low NO, the ratio of the concentrations of C₁₀H₁₅O_{*x*}• to C₁₀H₁₇O_{*x*}• was 0.61, and the ratios of the concentrations of C₁₀H₁₅O_{*x*}•-related termination products carbonyls (C₁₀H₁₄O_{*x*}) and organic nitrates (C₁₀H₁₅NO_{*x*}) to C₁₀H₁₇O_{*x*}•-related termination products carbonyls (C₁₀H₁₆O_{*x*}) and organic nitrates (C₁₀H₁₇NO_{*x*}) are 0.78 and 0.61, respectively (Fig. 3c). At high NO, the ratio of the concentrations of C₁₀H₁₅O_{*x*}• to C₁₀H₁₇O_{*x*}• was ~ 1.1 (Fig. 3), and the corresponding ratios of the concentrations of C₁₀H₁₅O_{*x*}•-related termination products to C₁₀H₁₇O_{*x*}•-related termination products are 0.82 and 0.53, respectively (Fig. 3c). Note that C₁₀H₁₆O_{*x*} can be termination products from either C₁₀H₁₅O_{*x*}• or C₁₀H₁₇O_{*x*}• radicals, depending on whether they contain hydroxyl or hydroperoxyl (ROH/ROOH) or carbonyl (RC=O) functionalities; the relative substituent contributions in C₁₀H₁₆O_{*x*} were quantified, using the method described in Sect. 2.2. The concentrations of C₁₀H₁₆O_{*x*} and C₁₀H₁₈O_{*x*} (alcohol and hydroperoxide products), formed from C₁₀H₁₅O_{*x*}• and C₁₀H₁₇O_{*x*}• radicals, respectively, were found to be negligible, and we can assign C₁₀H₁₆O_{*x*} products as carbonyls formed from the OH addition C₁₀H₁₇O_{*x*}• radicals. The NO_{*x*} dependence on C₁₀H₁₅O_{*x*}•/C₁₀H₁₇O_{*x*}• may be attributed to the differences in their reactivity. One explanation for the NO_{*x*} dependence is that the autoxidation of C₁₀H₁₅O_{*x*}• RO₂ rad-



Scheme 2. Example reaction scheme for HOM formation after H abstraction in limonene, based mostly on SAR prediction and starting at the fastest of the five allylic H-abstraction sites.

icals may be faster than that of $\text{C}_{10}\text{H}_{17}\text{O}_x \cdot$ RO₂ radicals, which leads to the lower concentration of $\text{C}_{10}\text{H}_{15}\text{O}_x \cdot$ at high NO and thus higher sensitivity to NO concentrations. Ratios of $\text{C}_{10}\text{H}_{16}\text{O}_x(\text{R}-\text{OH}/\text{OOH})/\text{C}_{10}\text{H}_{15}\text{O}_x \cdot$ can be derived with 0.47 and 0.02 at low and high NO, respectively. The decrease in $\text{C}_{10}\text{H}_{16}\text{O}_x(\text{R}-\text{OH}/\text{OOH})/\text{C}_{10}\text{H}_{15}\text{O}_x \cdot$ at high NO compared to low NO was more evident than the decrease in $\text{C}_{10}\text{H}_{18}\text{O}_x/\text{C}_{10}\text{H}_{17}\text{O}_x \cdot$. Theoretically, though, they should be similar. The difference may be attributed to the shift in $\text{C}_{10}\text{H}_{15}\text{O}_x \cdot$ distribution with a different number of O atoms, as evident in Fig. S6, and different isomers at high NO compared to low NO. At high NO, there might thus be more $\text{C}_{10}\text{H}_{15}\text{O}_x \cdot$ that reacts slower with HO₂ or has a lower branching ratio that forms ROOH in RO₂+HO₂, which depends on the explicit RO₂ structure, or has a lower yield that forms ROH in RO₂ plus RO₂. Overall, the

$\text{C}_{10}\text{H}_{15}\text{O}_x \cdot$ -related products formed via the H-abstraction channel contribute 41 % and 42 % of C₁₀ HOM monomer, respectively, at low and high NO. The ratio between the products of $\text{C}_{10}\text{H}_{15}\text{O}_x \cdot$ and $\text{C}_{10}\text{H}_{17}\text{O}_x \cdot$ radicals is stable at both low and high NO (Fig. 4), except for a small decrease at the early reaction times under low NO conditions (Fig. 4c), albeit with large error. At the same time, the nitrate ratio $\text{C}_{10}\text{H}_{15}\text{NO}_x/\text{C}_{10}\text{H}_{17}\text{NO}_x$ is lower than that of $\text{C}_{10}\text{H}_{14}\text{O}_x/\text{C}_{10}\text{H}_{16}\text{O}_x$, which indicates that carbonyl production from $\text{C}_{10}\text{H}_{15}\text{O}_x \cdot$ is more efficient than from $\text{C}_{10}\text{H}_{17}\text{O}_x \cdot$. The concentration of peroxy radicals $\text{C}_{10}\text{H}_{15}\text{O}_x \cdot$ and the related termination products $\text{C}_{10}\text{H}_{14}\text{O}_x$ and $\text{C}_{10}\text{H}_{15}\text{NO}_x$ were comparable to $\text{C}_{10}\text{H}_{17}\text{O}_x \cdot$ and its corresponding products, illustrating the significant role of the H-abstraction pathway in the HOM formation from the limonene oxidation by OH at low and high NO. The much higher abundance of carbonyl

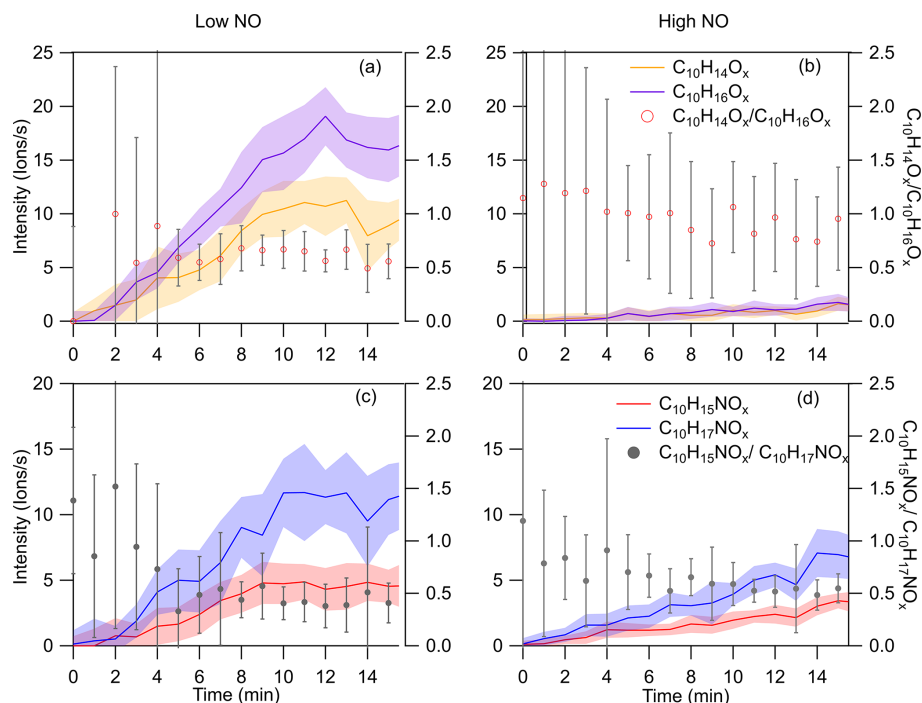


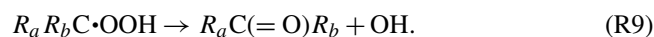
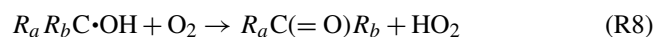
Figure 4. Time series of $C_{10}H_{15}O_x$ • and $C_{10}H_{17}O_x$ •-related families of carbonyls and organic nitrates during the first 15 min of the experiments. The carbonyl families $C_{10}H_{14}O_x$ (yellow), $C_{10}H_{16}O_x$ (purple), and their concentration ratio ($C_{10}H_{14}O_x/C_{10}H_{16}O_x$) are shown for (a) low and (b) high NO experiments. Time series for organic nitrate families $C_{10}H_{15}NO_x$ (red) and $C_{10}H_{17}NO_x$ (blue) and the concentration ratio of $C_{10}H_{15}NO_x/C_{10}H_{17}NO_x$, are similarly demonstrated in panel (c) for low NO experiments and panel (d) for high NO experiments. All data are averaged to 1 min, and the error bar represents 1 standard deviation.

than alcohol is unlikely to be explained by the RO plus O_2 forming carbonyl because, for large CO (C_{10} in this study), the RO plus O_2 is generally slower than unimolecular reactions, including H shift isomerization (i.e., alkoxy-peroxy pathway) and decomposition. The higher abundance of carbonyl products compared to alcohol products indicates that here a large fraction of the carbonyls is not formed from RO_2 plus RO_2 reactions (see also Fig. S3) but rather from termination reactions in $HOOQOO$ • radicals eliminating an OH radical after an α -OOH H atom migration, thus forming $O = QOOH$. This observation is in agreement with recent findings for α -pinene (Shen et al., 2022) and previous studies (Miller et al., 2005; Taatjes, 2006; Rissanen et al., 2014; Bianchi et al., 2019).

The large contribution of $C_{10}H_{15}O_x$ •-related products to HOM formation can be attributed to the significant contribution of H abstraction by OH in the initial step. While OH addition is believed to be the major initiation channel in the reaction of limonene plus OH, and H abstraction is often ignored in current chemical mechanisms (e.g., MCM v3.3.1), H abstraction by OH is clearly not negligible. Already previous studies have suggested that H abstraction can be a significant reaction pathway, with $\sim 34 \pm 8\%$ branching ratio for the reactions of limonene with OH radical at 298 K (Rio et al., 2010; Dash and Rajakumar, 2015) and

$33.6 \pm 4.8\%$ at 293 K (Braure et al., 2014). We found that the ratio of $C_{10}H_{15}O_x$ • to $C_{10}H_{17}O_x$ • at high NO conditions was higher than 2, emphasizing the importance of H abstraction. A similar abundance of carbonyls ($C_{10}H_{14}O_x$) and organic nitrates ($C_{10}H_{15}NO_x$) stemming from $C_{10}H_{15}O_x$ • radicals compared to their counterparts $C_{10}H_{16}O_x$ and $C_{10}H_{17}NO_x$ from $C_{10}H_{17}O_x$ • at both low and high NO levels (Fig. 3) likewise indicates that H abstraction in the first step of the limonene oxidation by OH is important for the subsequent oxidation. Moreover, the high relative yields of HOMs from the H-abstraction channel compared to its contribution in the limonene plus OH initiation reaction can be tentatively attributed to the difference in the autoxidation mechanisms (Schemes 1 and 2). Many of the autoxidation channels following the OH addition lead efficiently to termination products (Scheme 1) and require additional OH reactions to undergo further oxidation, whereas the RO_2 formed from H abstraction readily lend themselves to a sequence of O_2 additions once the ring structure is broken. The key difference is the presence of β -OH and β -OOH moieties in the alkoxy in the OH addition branch, which can form α -OH alkyl radicals and α -OOH alkyl radicals in fragmentation steps and further lead to HO_2 formation from α -OH alkyl radicals plus O_2 (Reaction R8) or by the regeneration of OH from α -OOH alkyl radicals (Reaction R9), thus preventing ring breaking

without termination of the autoxidation chain, as follows:



In contrast, the alkoxy step after H abstraction breaks the six-membered ring to a new RO₂, thereby enhancing autoxidation (Scheme 2). The propensity of the RO₂ from OH adducts to terminate the autoxidation chain, especially at higher NO, where β-OH and β-OOH alkoxy decomposition is prevalent, then allows the H-abstraction RO₂ to play a more dominant role. Contrary to our earlier studies on β-pinene or limonene with NO₃ (Shen et al., 2021; Guo et al., 2022), where we were able to assign RO₂ and products to first-, second-, or later-generation chemistry, no such clear *n*th-generation distinction can be made for the HOM mass spectrum traces in the limonene plus OH system. This suggests that the observed HOMs are a mixture formed in several generations of OH initiation reactions and lends further credence to our proposal that termination reactions requiring additional OH reactions are hampering the main OH addition channel from efficiently producing HOMs.

To our knowledge, no previous studies have observed C₁₀H₁₅O_x• radicals in limonene oxidation by OH, although in ozonolysis the formation of C₁₀H₁₅O_x• and their termination products, including C₁₀H_{14–16}O_{6–10} monomers and C_{18–20}H_{28–34}O_{6–16}, was observed (Hammes et al., 2019; Tomaz et al., 2021), and field observations have shown the presence of C₁₀H₁₅O_x• radicals in the atmosphere (Yan et al., 2020; Massoli et al., 2018). Recent theoretical work from Piletic and Kleindienst (2022) concluded that H abstraction does not contribute to HOMs in limonene plus OH, but this study did not account for any alkoxy-peroxy autoxidation steps. Our study, then, shows for the first time that H abstraction significantly contributes to HOM formation in the reaction of limonene plus OH under reaction conditions that allow the formation of alkoxy radicals, such as by reaction with NO, RO₂, or NO₃, as commonly found in the atmosphere.

Currently, an absolute calibration using HOM standards is not possible, mainly due to the difficulty of synthesizing pure HOMs and the unclear chemical structures of many HOMs. However, we think that it is reasonable to expect a generally similar sensitivity for HOMs in this study for the following reasons. First, Hyttinen et al. (2017) found that the increase in binding energy with NO₃[−] for molecules with an additional hydroperoxy group to two hydrogen bond donor functional groups is small for the HOMs formed in cyclohexene ozonolysis. As HOMs in this study generally contain more than two hydrogen bond donor functional groups, their sensitivity is expected to be similar. We used a unified H₂SO₄-based calibration coefficient for HOMs, which is commonly used to calibrate NO₃[−] CIMS (Kirkby et al., 2016; Jokinen et al., 2015; Rissanen et al., 2014; Ehn et al., 2014). Second, although the underestimation of certain

HOM-RO₂ formed from the α-pinene plus OH reaction has been reported (Berndt et al., 2016), such an underestimation was mainly attributed to the steric hindrance in forming a HOM–nitrate cluster for HOMs with bicyclic structures (C₁₀H₁₇O₇•; Berndt et al., 2016; see Sect. 3.2 of their Supplement), and thus, such underestimation is not common for all HOMs. In our study, we found the significance of the C₁₀H₁₅O_x•-related product at all oxygen contents, particularly for closed-shell products with the number of oxygen atoms being greater than eight, which is indicative of more H-donating functional groups (Fig. S6). This indicates that the significance of C₁₀H₁₅O_x•-related products is not affected by the detection sensitivity, which would mostly affect the sensitivity of less oxygenated compounds. And the presence of NO, particularly at high NO, leads to ring opening reactions, as shown in Scheme 1. Therefore, the HOM products from OH addition in this study are likely to form stable clusters with nitrate and thus have similar sensitivity with the HOMs formed via H abstraction in nitrate CIMS. Third, our previous study showed that using a unified sensitivity of H₂SO₄ only leads to a maximum uncertainty of a factor of 2 by comparing the condensation of HOMs and corresponding increase in aerosol mass (Pullinen et al., 2020). If for some currently unknown reason C₁₀H₁₇O_x•-related products had a higher sensitivity than the C₁₀H₁₅O_x•-related products, then this would lead us to underestimate of the significance of the OH H-abstraction pathway. This will not change our conclusion that the C₁₀H₁₅O_x•-related products contribute significantly to HOM formation.

We have further estimated the uncertainty in the fraction of C₁₀H₁₅O_x•-related products in C₁₀-HOM that resulted from the allocation of carbonyls and alcohols in C₁₀H₁₆O_x in Eqs. (2)–(8). The contributions of C₁₀H₁₅O_x•-related products range from 39.5 % to 41.4 % at low NO and 42.2 % to 42.6 % at high NO, respectively. We found that fraction of C₁₀H₁₅O_x•-related products in C₁₀-HOM was not affected much by how carbonyls and alcohols in C₁₀H₁₆O_x are allocated.

3.3.4 Comparison against α-pinene HOM formation

In our previous study, we observed the large contribution of H abstraction OH to HOM formation in the oxidation of α-pinene by OH (Shen et al., 2022). There, at low NO (0.03–0.1 ppb), the ratio of HOMs formed from H abstraction relative to OH addition increased at the beginning of the experiment and had a delay of 3–5 min before reaching 1 : 1. At high NO (~ 17 ppb), an enhancement of the HOM yields formed through H abstraction was observed, which was both absolute and relative to the HOMs formed through OH addition. Alkoxy radical steps were found to be a prerequisite for the autoxidation and thus HOM formation in the hydrogen abstraction pathway. As discussed in Sect. 3.3.3, in limonene plus OH oxidation, the ratios of C₁₀H₁₄O_x to C₁₀H₁₆O_x and of C₁₀H₁₅NO_x to C₁₀H₁₇NO_x and the time series of the ra-

tios were similar at low and high NO. These results indicate that the rate of autoxidation for both the limonene H abstraction and OH addition channels are affected to a similar extent by competing bimolecular reactions such as with NO. This contrasts with the enhancement of the HOM yield through H abstraction in the α -pinene system with increasing NO concentrations (Shen et al., 2022).

The different kinetic behavior relative to competing reactions can be attributed to the different molecular structures of α -pinene and limonene. α -pinene is a bicyclic rigid molecule, and the RO₂ formed from H abstraction do not undergo autoxidation, as the rate coefficients are $\leq 10^{-4} \text{ s}^{-1}$ (Shen et al., 2022). Even after breaking the first ring in an alkoxy step, autoxidation rates remain fairly slow, $\leq 10^{-1} \text{ s}^{-1}$, requiring a second alkoxy step with ring breaking before fast autoxidation occurs. This makes HOM formation through H abstraction sensitive to the NO concentration in the first few steps. In contrast, limonene has only a single six ring, and only a single alkoxy ring breaking is needed to allow fast autoxidation in the resulting non-cyclic molecule. Moreover, the primary RO₂ from the H abstraction of limonene can still undergo some slow autoxidation, with rates of $\sim 10^{-2} \text{ s}^{-1}$ (see Table 1), and possibly break the ring at a later stage (see Scheme 2). Overall, then, autoxidation in the limonene system after H abstraction is more competitive, even at lower NO than in the α -pinene system. We should note, though, that the low NO experiments of limonene oxidation were performed at NO concentrations that were higher by a factor of 2 to 7 compared to the low NO experiment for α -pinene (~ 0.2 and 0.03 – 0.1 ppb, respectively); we speculate that an NO dependence on the ratio of HOMs that formed via H abstraction versus OH addition might even become apparent in the limonene system at strongly reduced NO levels. The higher absolute contribution of HOMs from the H-abstraction channel in limonene (H-abstraction-related HOM yields are 0.77 % low NO and 0.10 % at high NO, as shown in Sect. 3.4) is also affected by the higher branching ratio of H abstraction in limonene plus OH, ~ 34 % (Rio et al., 2010; Dash and Rajakumar, 2015), compared to α -pinene plus OH, ~ 11 % (Vereecken and Peeters, 2000).

3.4 HOM yield

The HOM molar yields during the first 60 min were estimated to be $1.97^{+2.52}_{-1.06}$ % and $0.29^{+0.38}_{-0.16}$ % at low and high NO, respectively. In brief, the uncertainty (-54 %/+128 %) was estimated from the HOM signal intensity, VOC concentration, and calibration coefficient of H₂SO₄, as discussed by Zhao et al. (2021; see Sect. S1 in the Supplement). It is noted that the HOM yield is not very sensitive to the vapor wall loss rate, since HOM yields only change 11 % to -6 % upon a 100 % increase and 50 % decrease in wall loss rate (Zhao et al., 2021). We further note that these HOM yields may be subject to uncertainties due to the assumption that HOMs have the same sensitivity as H₂SO₄, as we

discussed in Sect. 3.3.3. As mentioned above, our previous study showed that using a unified sensitivity of H₂SO₄ only leads to a maximum uncertainty (that is a factor of 2) by comparing the condensation HOMs and corresponding increase in aerosol mass (Pullinen et al., 2020). The lower HOM yields at high NO can be partly attributed to the lower fractions of dimer products for the inhibitory effect of NO_x, as discussed previously (Sect. 3.2.3). Within the uncertainty, the HOM yield at high NO in this study is comparable to the HOM yield (0.93 ± 0.47) % from the photooxidation of limonene in a previous study (Jokinen et al., 2015). The difference in yield at low NO from Jokinen et al. (2015) may be attributed to different experimental methods and conditions. For example, Jokinen et al. (2015) derived the HOM yield from OH oxidation indirectly by comparing the HOM yield in ozonolysis with and without the OH scavenger, while in this study, we determined the HOM yield directly for the oxidation of limonene by OH. In ozonolysis, the cross-reactions of RO₂ that formed from ozonolysis and OH oxidation may produce accretion products, thus possibly confounding the results. By directly measuring the HOM yield in the oxidation of limonene by OH, such an influence is avoided. The NO concentration might be also different between our study and that of Jokinen et al. (2015). Additionally, the HOM molar yields related to H abstraction were further determined to be $0.77^{+0.98}_{-0.41}$ % at low NO and $0.10^{+0.13}_{-0.05}$ % at high NO, when assuming that the ratio of all HOMs from H abstraction to those from OH addition is equal to the corresponding ratio for C₁₀ monomers.

4 Conclusions and atmospheric implications

In this study, the HOM products in the oxidation of limonene with OH were investigated by using a NO₃⁻ CIMS with SAPHIR at Forschungszentrum Jülich. A large number of HOM monomers (C_{6–10}) and dimers (C_{17–20}) was detected and classified according to the number of carbon atoms. Among HOM products, the proportion of HOM monomers is far higher than dimers in both low and high NO conditions. C₁₀ HOMs were the most abundant monomers at both low and high NO. At low NO, the fraction of organic nitrates (31 %) was lower than that of non-nitrate HOMs (69 %). At high NO, a higher fraction of 41 % was observed for organic nitrates. Two major RO₂ radical families, C₁₀H₁₅O_x• and C₁₀H₁₇O_x•, were identified. While C₁₀H₁₇O_x• were formed via OH addition to a double bond, C₁₀H₁₅O_x• is proposed to be formed via H abstraction by OH on the basis of its molecular formula and the available literature. Although the concentrations of C₁₀H₁₅O_x•-related products were less than C₁₀H₁₇O_x•-related products, they remained at a comparable magnitude (38.9 % vs. 55.0 % at low NO and 33.7 % vs. 49.7 % at high NO). The formation pathways of C₁₀H₁₅O_x• and C₁₀H₁₇O_x• were proposed on the basis of observed signal intensity, theoretical kinetic calcu-

lations, and structure–activity relationships (SARs) for autoxidation. At both low and high NO, H abstraction by OH contributes a significant fraction of HOMs (41 % and 42 % of C₁₀ HOM monomer, respectively), demonstrating that H abstraction is important to the formation of HOMs in the oxidation of limonene with OH radical and contributes more than expected, given the ~34 % contribution in the initiation reaction. The key mechanistic difference between OH addition and H-abstraction pathways is that the former does not readily lead to breaking of the six-membered ring without chain termination, whereas H abstraction leads to fast first-generation autoxidation after an alkoxy-peroxy ring-breaking step. C₆–C₉ monomers are proposed to be formed via the fragmentation of alkoxy radicals, and C₁₇–C₂₀ dimers are proposed to be formed via accretion reactions.

The molar yields of total HOMs are estimated to be 1.97^{+2.52}_{-1.06} % and 0.29^{+0.38}_{-0.16} % in low and high NO conditions. Although the HOM yields in the oxidation of limonene with OH in this study are lower than that in the ozonolysis of limonene (Jokinen et al., 2015), the corresponding SOA mass yields (assuming the irreversible condensation of HOMs) can be as high as 4.3 % and 0.6 % at low NO and high NO, respectively. Similarly, while the gas-phase dimers observed in this study are clearly lower than the monomers in abundance, dimers may also be very efficient at condensing onto newly formed particles due to their large size and low volatility. These HOM dimer products are known to have an extremely low volatility due to their size and high degree of oxidation (Tröstl et al., 2016). At 17 ppb NO, the RO₂ fate is exclusively a reaction with NO and is representative of all environments in which the RO₂ loss is dominated by the reaction with NO. Such an environment includes urban regions and suburban regions, especially in developing countries such as East Asia and South Asia, where our HOM yield can be used to model these areas. In contrast, our HOM yield at low NO is representative of a rural and remote continental environment (Rohrer et al., 1998; Lelieveld et al., 2008; Whalley et al., 2011; Moiseenko et al., 2021; Wei et al., 2019). Combined, our results can thus be used directly in atmospheric chemical transport models to simulate the HOM concentrations in many atmospheric regimes (Pye et al., 2019; Xu et al., 2022) and help refine the simulations to assess its importance in new particle formation and particle growth (Zhao et al., 2020).

This study highlights the importance of the pathway of H abstraction by OH in competition with the OH addition to double bonds in the same molecule, at least for HOM formation, which has largely been neglected in current chemical mechanisms. The importance of the H-abstraction pathway to HOM formation also in the α -pinene plus OH oxidation has been shown in our recent study (Shen et al., 2022) and in recent experimental work by Williams et al. (2022). H abstraction in the case of limonene plus OH is more prominent than for α -pinene plus OH, but the OH abstraction pathway is important in both systems, suggesting its importance in

other terpenes or even other unsaturated species. We propose that, in order to accurately simulate HOM formation from the oxidation of limonene by OH, H abstraction should be considered in the chemical mechanisms of atmospheric models. Considering the key role HOMs in SOA particle formation and growth, this study further enables a more accurate simulation of the chemical composition and concentrations of SOA, in addition to the growth of particles to the cloud condensation nuclei (CCN) size in order to assess the impact of SOA on climate.

The experiments in this study were conducted at ambient relevant conditions by using limonene and OH concentrations at ambient levels and using natural sunlight. The major RO₂ loss rate in all experiments is via RO₂ plus NO. Therefore, the HOM composition and formation pathway can represent a large part of the daytime continental environment. The low NO conditions are representative of forested regions with biogenic monoterpene emissions and are influenced by anthropogenic emissions and of rural regions. The experiments at high NO in this study are relevant for the reactions of limonene with OH in urban environment, as limonene is also a major component of VCP besides the biogenic sources (Nazaroff and Weschler, 2004; Rossignol et al., 2013; Waring, 2016; Gkatzelis et al., 2021).

The fraction of organic nitrate HOMs, such as C₁₀H₁₅NO_x and C₁₀H₁₇NO_x, was significant in the total HOM products in both the low and high NO conditions examined, highlighting the importance of organic nitrates (ONs). Even at ~0.2 ppb NO, ONs account for a large part (31 %) of HOMs. ONs are important in the atmosphere, as they can serve as an NO_x reservoir (Ng et al., 2017). Highly functionalized ONs have been inferred to be capable of strongly partitioning to the particle phase (Perraud et al., 2012; Ng et al., 2007). The significant amounts of monoterpene-derived ONs that were observed in field campaigns (Massoli et al., 2018; Huang et al., 2019; Lee et al., 2016) indicate that ONs make up a significant fraction of SOA. The abundant presence of ONs highlights the importance of NO_x-driven chemistry in daytime. In most of the continental environment influenced by monoterpenes, ONs then likely contribute a large fraction of HOMs and SOA and contribute the organic nitrates and particle formation in the atmosphere.

Data availability. The Supplement provides additional figures and tables and further information on the CIMS calibration and HOM monomers and dimers with reduced carbon number.

The quantum chemical data (geometries, vibrational wavenumbers, rotational constants, energies, and partition functions) can be found at <https://doi.org/10.26165/JUELICH-DATA/9JVHEK> (Vereecken, 2023).

Supplement. The supplement related to this article is available online at: <https://doi.org/10.5194/acp-23-7297-2023-supplement>.

Author contributions. DZ and TFM designed the study. IP, HF, and DZ carried out instrument deployment and operation. HL analyzed the MS data and did the MCM simulation with the aid of DZ, HS. HL, DZ, TFM, and LV interpreted the compiled data set. LV performed the theoretical calculations and examined the reaction schemes. HL, DZ, TFM, and LV wrote the paper, and HS, IP, SK, LV, HF edited the paper. All the co-authors discussed the results and commented on the paper.

Competing interests. The contact author has declared that none of the authors has any competing interests.

Disclaimer. Publisher's note: Copernicus Publications remains neutral with regard to jurisdictional claims in published maps and institutional affiliations.

Acknowledgements. Hao Luo, Hongru Shen, and Defeng Zhao would like to thank the funding support of the Science and Technology Commission of Shanghai Municipality (grant no. 20230711400), National Natural Science Foundation of China (grant no. 41875145), Shanghai International Science and Technology Partnership Project (grant no. 21230780200), and Tibet University–Fudan Joint Laboratory for Biodiversity and Global Change. Sungah Kang, Astrid Kiendler-Scharr, and Thomas F. Mentel acknowledge the support by the EU Project FORCeS (grant no. 821205).

Financial support. This research has been supported by the Science and Technology Commission of Shanghai Municipality (grant no. 20230711400), National Natural Science Foundation of China (grant no. 41875145), Shanghai International Science and Technology Partnership Project (grant no. 21230780200), and the Horizon 2020 Framework Programme, H2020 European Institute of Innovation and Technology (grant no. 821205).

Review statement. This paper was edited by Ivan Kourtchev and reviewed by two anonymous referees.

References

- Alecu, I. M., Zheng, J., Zhao, Y., and Truhlar, D. G.: Computational thermochemistry: scale factor databases and scale factors for vibrational frequencies obtained from electronic model chemistries, *J. Chem. Theor. Comput.*, 6, 2872–2887, <https://doi.org/10.1021/ct100326h>, 2010.
- Bartlett, R. J. and Purvis, G. D.: Many-Body Perturbation-Theory, Coupled-Pair Many-Electron Theory, and Importance of Quadruple Excitations for Correlation Problem, *Int. J. Quant. Chem.*, 14, 561–581, <https://doi.org/10.1002/qua.560140504>, 1978.
- Berndt, T.: Peroxy Radical Processes and Product Formation in the OH Radical-Initiated Oxidation of α -Pinene for Near-Atmospheric Conditions, *J. Phys. Chem. A*, 125, 9151–9160, <https://doi.org/10.1021/acs.jpca.1c05576>, 2021.
- Berndt, T., Richters, S., Jokinen, T., Hyttinen, N., Kurtén, T., Otkjær, R. V., Kjaergaard, H. G., Stratmann, F., Herrmann, H., Sipilä, M., Kulmala, M., and Ehn, M.: Hydroxyl radical-induced formation of highly oxidized organic compounds, *Nat. Commun.*, 7, 13677, <https://doi.org/10.1038/ncomms13677>, 2016.
- Berndt, T., Mentler, B., Scholz, W., Fischer, L., Herrmann, H., Kulmala, M., and Hansel, A.: Accretion Product Formation from Ozonolysis and OH Radical Reaction of α -Pinene: Mechanistic Insight and the Influence of Isoprene and Ethylene, *Environ. Sci. Technol.*, 52, 11069–11077, <https://doi.org/10.1021/acs.est.8b02210>, 2018a.
- Berndt, T., Scholz, W., Mentler, B., Fischer, L., Herrmann, H., Kulmala, M., and Hansel, A.: Accretion Product Formation from Self- and Cross-Reactions of RO₂ Radicals in the Atmosphere, *Angew. Chem. Int. Ed. Engl.*, 57, 3820–3824, <https://doi.org/10.1002/anie.201710989>, 2018b.
- Bianchi, F., Kurtén, T., Riva, M., Mohr, C., Rissanen, M. P., Roldin, P., Berndt, T., Crouse, J. D., Wennberg, P. O., Mentel, T. F., Wildt, J., Junninen, H., Jokinen, T., Kulmala, M., Worsnop, D. R., Thornton, J. A., Donahue, N., Kjaergaard, H. G., and Ehn, M.: Highly Oxygenated Organic Molecules (HOM) from Gas-Phase Autoxidation Involving Peroxy Radicals: A Key Contributor to Atmospheric Aerosol, *Chem. Rev.*, 119, 3472–3509, <https://doi.org/10.1021/acs.chemrev.8b00395>, 2019.
- Braure, T., Bedjanian, Y., Romanias, M. N., Morin, J., Riffault, V., Tomas, A., and Coddeville, P.: Experimental study of the reactions of limonene with OH and OD radicals: kinetics and products, *J. Phys. Chem. A*, 118, 9482–9490, <https://doi.org/10.1021/jp507180g>, 2014.
- Chen, X. and Hopke, P. K.: A chamber study of secondary organic aerosol formation by limonene ozonolysis, *Indoor Air*, 20, 320–328, <https://doi.org/10.1111/j.1600-0668.2010.00656.x>, 2010.
- Crouse, J. D., Nielsen, L. B., Jørgensen, S., Kjaergaard, H. G., and Wennberg, P. O.: Autoxidation of Organic Compounds in the Atmosphere, *J. Phys. Chem. Lett.*, 4, 3513–3520, <https://doi.org/10.1021/jz4019207>, 2013.
- Dash, M. R. and Rajakumar, B.: Theoretical investigations of the gas phase reaction of limonene (C₁₀H₁₆) with OH radical, *Mol. Phys.*, 113, 3202–3215, <https://doi.org/10.1080/00268976.2015.1014002>, 2015.
- Dunning, T. H.: Gaussian basis sets for use in correlated molecular calculations. I. The atoms boron through neon and hydrogen, *J. Chem. Phys.*, 90, 1007–1023, <https://doi.org/10.1063/1.456153>, 1989.
- Dunning, T. H., Peterson, K. A., and Wilson, A. K.: Gaussian basis sets for use in correlated molecular calculations. X. The atoms aluminum through argon revisited, *J. Chem. Phys.*, 114, 9244–9253, <https://doi.org/10.1063/1.1367373>, 2001.
- Eckart, C.: The Penetration of a Potential Barrier by Electrons, *Phys. Rev.*, 35, 1303–1309, <https://doi.org/10.1103/PhysRev.35.1303>, 1930.
- Eddingsaas, N. C., Loza, C. L., Yee, L. D., Seinfeld, J. H., and Wennberg, P. O.: α -pinene photooxidation under controlled chemical conditions – Part 1: Gas-phase composition in low- and high-NO_x environments, *Atmos. Chem. Phys.*, 12, 6489–6504, <https://doi.org/10.5194/acp-12-6489-2012>, 2012.
- Ehn, M., Kleist, E., Junninen, H., Petäjä, T., Lönn, G., Schobesberger, S., Dal Maso, M., Trimborn, A., Kulmala, M., Worsnop, D. R., Wahner, A., Wildt, J., and Mentel, T. F.: Gas phase

- formation of extremely oxidized pinene reaction products in chamber and ambient air, *Atmos. Chem. Phys.*, 12, 5113–5127, <https://doi.org/10.5194/acp-12-5113-2012>, 2012.
- Ehn, M., Thornton, J. A., Kleist, E., Sipilä, M., Junninen, H., Pullinen, I., Springer, M., Rubach, F., Tillmann, R., Lee, B., Lopez-Hilfiker, F., Andres, S., Acir, I. H., Rissanen, M., Jokinen, T., Schobesberger, S., Kangasluoma, J., Kontkanen, J., Nieminen, T., Kurtén, T., Nielsen, L. B., Jørgensen, S., Kjaergaard, H. G., Canagaratna, M., Maso, M. D., Berndt, T., Petäjä, T., Wahner, A., Kerminen, V. M., Kulmala, M., Worsnop, D. R., Wildt, J., and Mentel, T. F.: A large source of low-volatility secondary organic aerosol, *Nature*, 506, 476–479, <https://doi.org/10.1038/nature13032>, 2014.
- Ehn, M., Berndt, T., Wildt, J., and Mentel, T.: Highly Oxygenated Molecules from Atmospheric Autoxidation of Hydrocarbons: A Prominent Challenge for Chemical Kinetics Studies, *Int. J. Chem. Kinet.*, 49, 821–831, <https://doi.org/10.1002/kin.21130>, 2017.
- Finlayson-Pitts, B. J. and Pitts, J. N. J.: *Chemistry of the Upper and Lower Atmosphere: Theory, Experiments, and Applications*, Academic Press, San Diego, San Francisco, New York, Boston, London, Sydney, Tokyo, ISBN 978-0-12-257060-5 <https://doi.org/10.1016/B978-0-12-257060-5.X5000-X>, 2000.
- Friedman, B. and Farmer, D. K.: SOA and gas phase organic acid yields from the sequential photooxidation of seven monoterpenes, *Atmos. Environ.*, 187, 335–345, <https://doi.org/10.1016/j.atmosenv.2018.06.003>, 2018.
- Frisch, M. J., Trucks, G. W., Schlegel, H. B., Scuseria, G. E., Robb, M. A., Cheeseman, J. R., Scalmani, G., Barone, V., Petersson, G. A., Nakatsuji, H., Li, X., Caricato, M., Marenich, A. V., Bloino, J., Janesko, B. G., Gomperts, R., Mennucci, B., Hratchian, H. P., Ortiz, J. V., Izmaylov, A. F., Sonnenberg, J. L., Williams-Young, D., Ding, F., Lipparini, F., Egidi, F., Goings, J., Peng, B., Petrone, A., Henderson, T., Ranasinghe, D., Zakrzewski, V. G., Gao, J., Rega, N., Zheng, G., Liang, W., Hada, M., Ehara, M., Toyota, K., Fukuda, R., Hasegawa, J., Ishida, M., Nakajima, T., Honda, Y., Kitao, O., Nakai, H., Vreven, T., Throssell, K., Montgomery, J. A., Jr., Peralta, J. E., Ogliaro, F., Bearpark, M. J., Heyd, J. J., Brothers, E. N., Kudin, K. N., Staroverov, V. N., Keith, T. A., Kobayashi, R., Normand, J., Raghavachari, K., Rendell, A. P., Burant, J. C., Iyengar, S. S., Tomasi, J., Cossi, M., Millam, J. M., Klene, M., Adamo, C., Cammi, R., Ochterski, J. W., Martin, R. L., Morokuma, K., Farkas, O., Foresman, J. B., and Fox, D. J.: Gaussian 09 Revision E.01, Gaussian, Inc., Wallingford CT, [code], <https://gaussian.com/gaussian16/> (last access: 28 June 2023), 2016.
- Fuchs, H., Bohn, B., Hofzumahaus, A., Holland, F., Lu, K. D., Nehr, S., Rohrer, F., and Wahner, A.: Detection of HO₂ by laser-induced fluorescence: calibration and interferences from RO₂ radicals, *Atmos. Meas. Tech.*, 4, 1209–1225, <https://doi.org/10.5194/amt-4-1209-2011>, 2011.
- Fuchs, H., Dorn, H.-P., Bachner, M., Bohn, B., Brauers, T., Gomm, S., Hofzumahaus, A., Holland, F., Nehr, S., Rohrer, F., Tillmann, R., and Wahner, A.: Comparison of OH concentration measurements by DOAS and LIF during SAPHIR chamber experiments at high OH reactivity and low NO concentration, *Atmos. Meas. Tech.*, 5, 1611–1626, <https://doi.org/10.5194/amt-5-1611-2012>, 2012.
- Gkatzelis, G. I., Coggon, M. M., McDonald, B. C., Peischl, J., Gilman, J. B., Aikin, K. C., Robinson, M. A., Canonaco, F., Prevot, A. S. H., Trainer, M., and Warneke, C.: Observations Confirm that Volatile Chemical Products Are a Major Source of Petrochemical Emissions in U.S. Cities, *Environ. Sci. Technol.*, 55, 4332–4343, <https://doi.org/10.1021/acs.est.0c05471>, 2021.
- Goerigk, L., Hansen, A., Bauer, C., Ehrlich, S., Najibi, A., and Grimme, S.: A look at the density functional theory zoo with the advanced GMTKN55 database for general main group thermochemistry, kinetics and noncovalent interactions, *Phys. Chem. Chem. Phys.*, 19, 32184–32215, <https://doi.org/10.1039/c7cp04913g>, 2017.
- Gong, Y., Chen, Z., and Li, H.: The oxidation regime and SOA composition in limonene ozonolysis: roles of different double bonds, radicals, and water, *Atmos. Chem. Phys.*, 18, 15105–15123, <https://doi.org/10.5194/acp-18-15105-2018>, 2018.
- Griffin, R. J., Cocker, D. R., Flagan, R. C., and Seinfeld, J. H.: Organic aerosol formation from the oxidation of biogenic hydrocarbons, *J. Geophys. Res.*, 104, 3555–3567, <https://doi.org/10.1029/1998jd100049>, 1999.
- Grimme, S., Ehrlich, S., and Goerigk, L.: Effect of the damping function in dispersion corrected density functional theory, *J. Comput. Chem.*, 32, 1456–1465, <https://doi.org/10.1002/jcc.21759>, 2011.
- Guenther, A. B., Jiang, X., Heald, C. L., Sakulyanontvittaya, T., Duhl, T., Emmons, L. K., and Wang, X.: The Model of Emissions of Gases and Aerosols from Nature version 2.1 (MEGAN2.1): an extended and updated framework for modeling biogenic emissions, *Geosci. Model Dev.*, 5, 1471–1492, <https://doi.org/10.5194/gmd-5-1471-2012>, 2012.
- Guo, Y., Shen, H., Pullinen, I., Luo, H., Kang, S., Vereecken, L., Fuchs, H., Hallquist, M., Acir, I.-H., Tillmann, R., Rohrer, F., Wildt, J., Kiendler-Scharr, A., Wahner, A., Zhao, D., and Mentel, T. F.: Identification of highly oxygenated organic molecules and their role in aerosol formation in the reaction of limonene with nitrate radical, *Atmos. Chem. Phys.*, 22, 11323–11346, <https://doi.org/10.5194/acp-22-11323-2022>, 2022.
- Hakola, H., Arey, J., Aschmann, S. M., and Atkinson, R.: Product Formation from the Gas-Phase Reactions of OH Radicals and O₃ with a Series of Monoterpenes, *J. Atmos. Chem.*, 18, 75–102, <https://doi.org/10.1007/Bf00694375>, 1994.
- Hallquist, M., Wenger, J. C., Baltensperger, U., Rudich, Y., Simpson, D., Claeys, M., Dommen, J., Donahue, N. M., George, C., Goldstein, A. H., Hamilton, J. F., Herrmann, H., Hoffmann, T., Iinuma, Y., Jang, M., Jenkin, M. E., Jimenez, J. L., Kiendler-Scharr, A., Maenhaut, W., McFiggans, G., Mentel, Th. F., Monod, A., Prévôt, A. S. H., Seinfeld, J. H., Surratt, J. D., Szmigielski, R., and Wildt, J.: The formation, properties and impact of secondary organic aerosol: current and emerging issues, *Atmos. Chem. Phys.*, 9, 5155–5236, <https://doi.org/10.5194/acp-9-5155-2009>, 2009.
- Hammes, J., Lutz, A., Mentel, T., Faxon, C., and Hallquist, M.: Carboxylic acids from limonene oxidation by ozone and hydroxyl radicals: insights into mechanisms derived using a FIGAERO-CIMS, *Atmos. Chem. Phys.*, 19, 13037–13052, <https://doi.org/10.5194/acp-19-13037-2019>, 2019.
- Huang, W., Saathoff, H., Shen, X., Ramisetty, R., Leisner, T., and Mohr, C.: Chemical Characterization of Highly Functionalized Organonitrates Contributing to Night-Time Organic Aerosol

- Mass Loadings and Particle Growth, *Environ. Sci. Technol.*, 53, 1165–1174, <https://doi.org/10.1021/acs.est.8b05826>, 2019.
- Hytinen, N., Rissanen, M. P., and Kurtén, T.: Computational Comparison of Acetate and Nitrate Chemical Ionization of Highly Oxidized Cyclohexene Ozonolysis Intermediates and Products, *J. Phys. Chem. A*, 121, 2172–2179, <https://doi.org/10.1021/acs.jpca.6b12654>, 2017.
- Jaoui, M., Corse, E., Kleindienst, T. E., Offenber, J. H., Lewandowski, M., and Edney, E. O.: Analysis of Secondary Organic Aerosol Compounds from the Photooxidation of d Limonene in the Presence of NO_x and their Detection in Ambient $\text{PM}_{2.5}$, *Environ. Sci. Technol.*, 40, 3819–3828, 2006.
- Jenkin, M. E., Saunders, S. M., and Pilling, M. J.: The tropospheric degradation of volatile organic compounds: a protocol for mechanism development, *Atmos. Environ.*, 31, 81–104, 1997.
- Jenkin, M. E., Valorso, R., Aumont, B., Rickard, A. R., and Wallington, T. J.: Estimation of rate coefficients and branching ratios for gas-phase reactions of OH with aliphatic organic compounds for use in automated mechanism construction, *Atmos. Chem. Phys.*, 18, 9297–9328, <https://doi.org/10.5194/acp-18-9297-2018>, 2018.
- Jenkin, M. E., Valorso, R., Aumont, B., and Rickard, A. R.: Estimation of rate coefficients and branching ratios for reactions of organic peroxy radicals for use in automated mechanism construction, *Atmos. Chem. Phys.*, 19, 7691–7717, <https://doi.org/10.5194/acp-19-7691-2019>, 2019.
- Johnston, H. S. and Heicklen, J.: Tunnelling Corrections for Unsymmetrical Eckart Potential Energy Barriers, *J. Phys. Chem.*, 66, 532–533, 1962.
- Jokinen, T., Sipilä, M., Richters, S., Kerminen, V. M., Paasonen, P., Stratmann, F., Worsnop, D., Kulmala, M., Ehn, M., Herrmann, H., and Berndt, T.: Rapid autoxidation forms highly oxidized RO_2 radicals in the atmosphere, *Angew. Chem. Int. Ed.*, 53, 14596–14600, <https://doi.org/10.1002/anie.201408566>, 2014.
- Jokinen, T., Berndt, T., Makkonen, R., Kerminen, V. M., Junninen, H., Paasonen, P., Stratmann, F., Herrmann, H., Guenther, A. B., Worsnop, D. R., Kulmala, M., Ehn, M., and Sipilä, M.: Production of extremely low volatility organic compounds from biogenic emissions: Measured yields and atmospheric implications, *P. Natl. Acad. Sci. USA*, 112, 7123–7128, <https://doi.org/10.1073/pnas.1423977112>, 2015.
- Jørgensen, S., Knap, H. C., Otkjær, R. V., Jensen, A. M., Kjeldsen, M. L., Wennberg, P. O., and Kjaergaard, H. G.: Rapid Hydrogen Shift Scrambling in Hydroperoxy-Substituted Organic Peroxy Radicals, *J. Phys. Chem. A*, 120, 266–275, <https://doi.org/10.1021/acs.jpca.5b06768>, 2016.
- Kanakidou, M., Seinfeld, J. H., Pandis, S. N., Barnes, I., Dentener, F. J., Facchini, M. C., Van Dingenen, R., Ervens, B., Nenes, A., Nielsen, C. J., Swietlicki, E., Putaud, J. P., Balkanski, Y., Fuzzi, S., Horth, J., Moortgat, G. K., Winterhalter, R., Myhre, C. E. L., Tsigaridis, K., Vignati, E., Stephanou, E. G., and Wilson, J.: Organic aerosol and global climate modelling: a review, *Atmos. Chem. Phys.*, 5, 1053–1123, <https://doi.org/10.5194/acp-5-1053-2005>, 2005.
- Kenseth, C. M., Huang, Y., Zhao, R., Dalleska, N. F., Hethcox, J. C., Stoltz, B. M., and Seinfeld, J. H.: Synergistic $\text{O}_3 + \text{OH}$ oxidation pathway to extremely low-volatility dimers revealed in beta-pinene secondary organic aerosol, *P. Natl. Acad. Sci. USA*, 115, 8301–8306, <https://doi.org/10.1073/pnas.1804671115>, 2018.
- Kirkby, J., Duplissy, J., Sengupta, K., Frege, C., Gordon, H., Williamson, C., Heinritzi, M., Simon, M., Yan, C., Almeida, J., Tröstl, J., Nieminen, T., Ortega, I. K., Wagner, R., Adamov, A., Amorim, A., Bernhammer, A. K., Bianchi, F., Breitenlechner, M., Brilke, S., Chen, X., Craven, J., Dias, A., Ehrhart, S., Flagan, R. C., Franchin, A., Fuchs, C., Guida, R., Hakala, J., Hoyle, C. R., Jokinen, T., Junninen, H., Kangasluoma, J., Kim, J., Krapf, M., Kürten, A., Laaksonen, A., Lehtipalo, K., Makhmutov, V., Mathot, S., Molteni, U., Onnela, A., Peräkylä, O., Piel, F., Petäjä, T., Praplan, A. P., Pringle, K., Rap, A., Richards, N. A., Riipinen, I., Rissanen, M. P., Rondo, L., Sarnela, N., Schobesberger, S., Scott, C. E., Seinfeld, J. H., Sipilä, M., Steiner, G., Stozhkov, Y., Stratmann, F., Tomé, A., Virtanen, A., Vogel, A. L., Wagner, A. C., Wagner, P. E., Weingartner, E., Wimmer, D., Winkler, P. M., Ye, P., Zhang, X., Hansel, A., Dommen, J., Donahue, N. M., Worsnop, D. R., Baltensperger, U., Kulmala, M., Carslaw, K. S., and Curtius, J.: Ion-induced nucleation of pure biogenic particles, *Nature*, 533, 521–526, <https://doi.org/10.1038/nature17953>, 2016.
- Knap, H. C. and Jørgensen, S.: Rapid Hydrogen Shift Reactions in Acyl Peroxy Radicals, *J. Phys. Chem. A*, 121, 1470–1479, <https://doi.org/10.1021/acs.jpca.6b12787>, 2017.
- Koch, S., Winterhalter, R., Uherek, E., Koloff, A., Neeb, P., and Moortgat, G. K.: Formation of new particles in the gas-phase ozonolysis of monoterpenes, *Atmos. Environ.*, 34, 4031–4042, 2000.
- Krechmer, J. E., Coggon, M. M., Massoli, P., Nguyen, T. B., Crouse, J. D., Hu, W., Day, D. A., Tyndall, G. S., Henze, D. K., Rivera-Rios, J. C., Nowak, J. B., Kimmel, J. R., Mauldin, R. L., Stark, H., Jayne, J. T., Sipilä, M., Junninen, H., Clair, J. M. S., Zhang, X., Feiner, P. A., Zhang, L., Miller, D. O., Brune, W. H., Keutsch, F. N., Wennberg, P. O., Seinfeld, J. H., Worsnop, D. R., Jimenez, J. L., and Canagaratna, M. R.: Formation of Low Volatility Organic Compounds and Secondary Organic Aerosol from Isoprene Hydroxyhydroperoxide Low-NO Oxidation, *Environ. Sci. Technol.*, 49, 10330–10339, <https://doi.org/10.1021/acs.est.5b02031>, 2015.
- Larsen, B. R., Di Bella, D., Glasius, M., Winterhalter, R., Jensen, N. R., and Hjorth, J.: Gas-phase OH oxidation of monoterpenes: Gaseous and particulate products, *J. Atmos. Chem.*, 38, 231–276, <https://doi.org/10.1023/A:1006487530903>, 2001.
- Lee, A., Goldstein, A. H., Kroll, J. H., Ng, N. L., Varutbangkul, V., Flagan, R. C., and Seinfeld, J. H.: Gas-phase products and secondary aerosol yields from the photooxidation of 16 different terpenes, *J. Geophys. Res.*, 111, D17305, <https://doi.org/10.1029/2006jd007050>, 2006a.
- Lee, A., Goldstein, A. H., Keywood, M. D., Gao, S., Varutbangkul, V., Bahreini, R., Ng, N. L., Flagan, R. C., and Seinfeld, J. H.: Gas-phase products and secondary aerosol yields from the ozonolysis of ten different terpenes, *J. Geophys. Res.*, 111, D07302, <https://doi.org/10.1029/2005jd006437>, 2006b.
- Lee, B. H., Mohr, C., Lopez-Hilfiker, F. D., Lutz, A., Hallquist, M., Lee, L., Romer, P., Cohen, R. C., Iyer, S., Kurtén, T., Hu, W., Day, D. A., Campuzano-Jost, P., Jimenez, J. L., Xu, L., Ng, N. L., Guo, H., Weber, R. J., Wild, R. J., Brown, S. S., Koss, A., de Gouw, J., Olson, K., Goldstein, A. H., Seco, R., Kim, S., McAvey, K., Shepson, P. B., Starn, T., Baumann, K., Edgerton, E. S., Liu, J., Shilling, J. E., Miller, D. O., Brune, W., Schobesberger, S., D'Ambro, E. L., and Thornton, J. A.:

- Highly functionalized organic nitrates in the southeast United States: Contribution to secondary organic aerosol and reactive nitrogen budgets, *P. Natl. Acad. Sci. USA*, 113, 1516–1521, <https://doi.org/10.1073/pnas.1508108113>, 2016.
- Lelieveld, J., Butler, T. M., Crowley, J. N., Dillon, T. J., Fischer, H., Ganzeveld, L., Harder, H., Lawrence, M. G., Martinez, M., Taraborrelli, D., and Williams, J.: Atmospheric oxidation capacity sustained by a tropical forest, *Nature*, 452, 737–740, <https://doi.org/10.1038/nature06870>, 2008.
- Massoli, P., Stark, H., Canagaratna, M. R., Krechmer, J. E., Xu, L., Ng, N. L., Mauldin, Ó., Roy, L., Yan, C., Kimmel, J., Misztal, P. K., Jimenez, J. L., Jayne, J. T., and Worsnop, D. R.: Ambient Measurements of Highly Oxidized Gas-Phase Molecules during the Southern Oxidant and Aerosol Study (SOAS) 2013, *ACS Earth Space Chem.*, 2, 653–672, <https://doi.org/10.1021/acsearthspacechem.8b00028>, 2018.
- Mayorga, R., Xia, Y., Zhao, Z., Long, B., and Zhang, H.: Peroxy Radical Autoxidation and Sequential Oxidation in Organic Nitrate Formation during Limonene Night-time Oxidation, *Environ. Sci. Technol.*, 56, 15337–15346, <https://doi.org/10.1021/acs.est.2c04030>, 2022.
- McFiggans, G., Mentel, T. F., Wildt, J., Pullinen, I., Kang, S., Kleist, E., Schmitt, S., Springer, M., Tillmann, R., Wu, C., Zhao, D., Hallquist, M., Faxon, C., Le Breton, M., Hallquist, Å. M., Simpson, D., Bergström, R., Jenkin, M. E., Ehn, M., Thornton, J. A., Alfarra, M. R., Bannan, T. J., Percival, C. J., Priestley, M., Topping, D., and Kiendler-Scharr, A.: Secondary organic aerosol reduced by mixture of atmospheric vapours, *Nature*, 565, 587–593, <https://doi.org/10.1038/s41586-018-0871-y>, 2019.
- Mentel, T. F., Springer, M., Ehn, M., Kleist, E., Pullinen, I., Kurtén, T., Rissanen, M., Wahner, A., and Wildt, J.: Formation of highly oxidized multifunctional compounds: autoxidation of peroxy radicals formed in the ozonolysis of alkenes – deduced from structure–product relationships, *Atmos. Chem. Phys.*, 15, 6745–6765, <https://doi.org/10.5194/acp-15-6745-2015>, 2015.
- Miller, J. A., Pilling, M. J., and Troe, J.: Unravelling combustion mechanisms through a quantitative understanding of elementary reactions, *P. Combust. Inst.*, 30, 43–88, <https://doi.org/10.1016/j.proci.2004.08.281>, 2005.
- Moiseenko, K. B., Vasileva, A. V., Skorokhod, A. I., Belikov, I. B., Repin, A. Y., and Shtabkin, Y. A.: Regional Impact of Ozone Precursor Emissions on NO_x and O₃ Levels at ZOTTO Tall Tower in Central Siberia, *Earth Space Sci.*, 8, e2021EA001762, <https://doi.org/10.1029/2021ea001762>, 2021.
- Møller, K. H., Bates, K. H., and Kjaergaard, H. G.: The Importance of Peroxy Radical Hydrogen-Shift Reactions in Atmospheric Isoprene Oxidation, *J. Phys. Chem. A*, 123, 920–932, <https://doi.org/10.1021/acs.jpca.8b10432>, 2019.
- Molteni, U., Simon, M., Heinritzi, M., Hoyle, C. R., Bernhammer, A.-K., Bianchi, F., Breitenlechner, M., Brilke, S., Dias, A., Duplissy, J., Frege, C., Gordon, H., Heyn, C., Jokinen, T., Kürten, A., Lehtipalo, K., Makhmutov, V., Petäjä, T., Pieber, S. M., Praplan, A. P., Schobesberger, S., Steiner, G., Stozhkov, Y., Tomé, A., Tröstl, J., Wagner, A. C., Wagner, R., Williamson, C., Yan, C., Baltensperger, U., Curtius, J., Donahue, N. M., Hansel, A., Kirkby, J., Kulmala, M., Worsnop, D. R., and Dommen, J.: Formation of Highly Oxygenated Organic Molecules from α -Pinene Ozonolysis: Chemical Characteristics, Mechanism, and Kinetic Model Development, *ACS Earth Space Chem.*, 3, 873–883, <https://doi.org/10.1021/acsearthspacechem.9b00035>, 2019.
- Nazaroff, W. W. and Weschler, C. J.: Cleaning products and air fresheners: exposure to primary and secondary air pollutants, *Atmos. Environ.*, 38, 2841–2865, <https://doi.org/10.1016/j.atmosenv.2004.02.040>, 2004.
- Ng, N. L., Chhabra, P. S., Chan, A. W. H., Surratt, J. D., Kroll, J. H., Kwan, A. J., McCabe, D. C., Wennberg, P. O., Sorooshian, A., Murphy, S. M., Dalleska, N. F., Flagan, R. C., and Seinfeld, J. H.: Effect of NO_x level on secondary organic aerosol (SOA) formation from the photooxidation of terpenes, *Atmos. Chem. Phys.*, 7, 5159–5174, <https://doi.org/10.5194/acp-7-5159-2007>, 2007.
- Ng, N. L., Brown, S. S., Archibald, A. T., Atlas, E., Cohen, R. C., Crowley, J. N., Day, D. A., Donahue, N. M., Fry, J. L., Fuchs, H., Griffin, R. J., Guzman, M. I., Herrmann, H., Hodzic, A., Iinuma, Y., Jimenez, J. L., Kiendler-Scharr, A., Lee, B. H., Luecken, D. J., Mao, J., McLaren, R., Mutzel, A., Osthoff, H. D., Ouyang, B., Picquet-Varrault, B., Platt, U., Pye, H. O. T., Rudich, Y., Schwantes, R. H., Shiraiwa, M., Stutz, J., Thornton, J. A., Tilgner, A., Williams, B. J., and Zaveri, R. A.: Nitrate radicals and biogenic volatile organic compounds: oxidation, mechanisms, and organic aerosol, *Atmos. Chem. Phys.*, 17, 2103–2162, <https://doi.org/10.5194/acp-17-2103-2017>, 2017.
- Novelli, A., Cho, C., Fuchs, H., Hofzumahaus, A., Rohrer, F., Tillmann, R., Kiendler-Scharr, A., Wahner, A., and Vereecken, L.: Experimental and theoretical study on the impact of a nitrate group on the chemistry of alkoxy radicals, *Phys. Chem. Chem. Phys.*, 23, 5474–5495, <https://doi.org/10.1039/d0cp05555g>, 2021.
- Nozière, B. and Vereecken, L.: Direct Observation of Aliphatic Peroxy Radical Autoxidation and Water Effects: An Experimental and Theoretical Study, *Angew. Chem. Int. Ed.*, 58, 13976–13982, <https://doi.org/10.1002/anie.201907981>, 2019.
- Pang, J. Y. S., Novelli, A., Kaminski, M., Acir, I.-H., Bohn, B., Carlsson, P. T. M., Cho, C., Dorn, H.-P., Hofzumahaus, A., Li, X., Lutz, A., Nehr, S., Reimer, D., Rohrer, F., Tillmann, R., Wegener, R., Kiendler-Scharr, A., Wahner, A., and Fuchs, H.: Investigation of the limonene photooxidation by OH at different NO concentrations in the atmospheric simulation chamber SAPHIR (Simulation of Atmospheric Photochemistry In a large Reaction Chamber), *Atmos. Chem. Phys.*, 22, 8497–8527, <https://doi.org/10.5194/acp-22-8497-2022>, 2022.
- Peeters, J., Vandenberk, S., Piessens, E., and Pultau, V.: H-atom abstraction in reactions of cyclic polyalkenes with OH, *Chemosphere*, 38, 1189–1195, 1999.
- Perraud, V., Bruns, E. A., Ezell, M. J., Johnson, S. N., Yu, Y., Alexander, M. L., Zelenyuk, A., Imre, D., Chang, W. L., Dabdub, D., Pankow, J. F., and Finlayson-Pitts, B. J.: Nonequilibrium atmospheric secondary organic aerosol formation and growth, *P. Natl. Acad. Sci. USA*, 109, 2836–2841, <https://doi.org/10.1073/pnas.1119909109>, 2012.
- Piletic, I. R. and Kleindienst, T. E.: Rates and Yields of Unimolecular Reactions Producing Highly Oxidized Peroxy Radicals in the OH-Induced Autoxidation of α -Pinene, β -Pinene, and Limonene, *J. Phys. Chem. A*, 126, 88–100, <https://doi.org/10.1021/acs.jpca.1c07961>, 2022.
- Praske, E., Otkjær, R. V., Crouse, J. D., Hethcox, J. C., Stoltz, B. M., Kjaergaard, H. G., and Wennberg, P. O.: Intramolecular Hydrogen Shift Chemistry of Hydroperoxy-

- Substituted Peroxy Radicals, *J. Phys. Chem. A*, 123, 590–600, <https://doi.org/10.1021/acs.jpca.8b09745>, 2019.
- Pullinen, I., Schmitt, S., Kang, S., Sarrafzadeh, M., Schlag, P., Andres, S., Kleist, E., Mentel, T. F., Rohrer, F., Springer, M., Tillmann, R., Wildt, J., Wu, C., Zhao, D., Wahner, A., and Kiendler-Scharr, A.: Impact of NO_x on secondary organic aerosol (SOA) formation from α -pinene and β -pinene photooxidation: the role of highly oxygenated organic nitrates, *Atmos. Chem. Phys.*, 20, 10125–10147, <https://doi.org/10.5194/acp-20-10125-2020>, 2020.
- Pye, H. O. T., D'Ambro, E. L., Lee, B., Schobesberger, S., Takeuchi, M., Zhao, Y., Lopez-Hilfiker, F., Liu, J. M., Shilling, J. E., Xing, J., Mathur, R., Middlebrook, A. M., Liao, J., Welti, A., Graus, M., Warneke, C., de Gouw, J. A., Holloway, J. S., Ryer-son, T. B., Pollack, I. B., and Thornton, J. A.: Anthropogenic enhancements to production of highly oxygenated molecules from autoxidation, *P. Natl. Acad. Sci. USA*, 116, 6641–6646, <https://doi.org/10.1073/pnas.1810774116>, 2019.
- Quéléver, L. L. J., Kristensen, K., Normann Jensen, L., Rosati, B., Teiwes, R., Daellenbach, K. R., Peräkylä, O., Roldin, P., Bossi, R., Pedersen, H. B., Glasius, M., Bilde, M., and Ehn, M.: Effect of temperature on the formation of highly oxygenated organic molecules (HOMs) from alpha-pinene ozonolysis, *Atmos. Chem. Phys.*, 19, 7609–7625, <https://doi.org/10.5194/acp-19-7609-2019>, 2019.
- Rio, C., Flaud, P. M., Loison, J. C., and Villenave, E.: Experimental reevaluation of the importance of the abstraction channel in the reactions of monoterpenes with OH radicals, *Chem. Phys. Chem.*, 11, 3962–3970, <https://doi.org/10.1002/cphc.201000518>, 2010.
- Rissanen, M. P., Kurtén, T., Sipilä, M., Thornton, J. A., Kangasluoma, J., Sarnela, N., Junninen, H., Jørgensen, S., Schallhart, S., Kajos, M. K., Taipale, R., Springer, M., Mentel, T. F., Ruuskanen, T., Petäjä, T., Worsnop, D. R., Kjaergaard, H. G., and Ehn, M.: The formation of highly oxidized multifunctional products in the ozonolysis of cyclohexene, *J. Am. Chem. Soc.*, 136, 15596–15606, <https://doi.org/10.1021/ja507146s>, 2014.
- Rohrer, F., Bruning, D., Grobler, E. S., Weber, M., Ehhalt, D. H., Neubert, R., Schussler, W., and Levin, I.: Mixing ratios and photochemical state of NO and NO_2 observed during the POP-COSTAR field campaign at a rural site in Germany, *J. Atmos. Chem.*, 31, 119–137, <https://doi.org/10.1023/A:1006166116242>, 1998.
- Rohrer, F., Bohn, B., Brauers, T., Brüning, D., Johnen, F.-J., Wahner, A., and Kleffmann, J.: Characterisation of the photolytic HONO-source in the atmosphere simulation chamber SAPHIR, *Atmos. Chem. Phys.*, 5, 2189–2201, <https://doi.org/10.5194/acp-5-2189-2005>, 2005.
- Romonosky, D. E., Laskin, A., Laskin, J., and Nizkorodov, S. A.: High-resolution mass spectrometry and molecular characterization of aqueous photochemistry products of common types of secondary organic aerosols, *J. Phys. Chem. A*, 119, 2594–2606, <https://doi.org/10.1021/jp509476r>, 2015.
- Rosignol, S., Rio, C., Ustache, A., Fable, S., Nicolle, J., Mème, A., D'Anna, B., Nicolas, M., Leoz, E., and Chiappini, L.: The use of a housecleaning product in an indoor environment leading to oxygenated polar compounds and SOA formation: Gas and particulate phase chemical characterization, *Atmos. Environ.*, 75, 196–205, <https://doi.org/10.1016/j.atmosenv.2013.03.045>, 2013.
- Saathoff, H., Naumann, K.-H., Möhler, O., Jonsson, Å. M., Hallquist, M., Kiendler-Scharr, A., Mentel, Th. F., Tillmann, R., and Schurath, U.: Temperature dependence of yields of secondary organic aerosols from the ozonolysis of α -pinene and limonene, *Atmos. Chem. Phys.*, 9, 1551–1577, <https://doi.org/10.5194/acp-9-1551-2009>, 2009.
- Shen, H., Zhao, D., Pullinen, I., Kang, S., Vereecken, L., Fuchs, H., Acir, I. H., Tillmann, R., Rohrer, F., Wildt, J., Kiendler-Scharr, A., Wahner, A., and Mentel, T. F.: Highly Oxygenated Organic Nitrates Formed from NO_3 Radical-Initiated Oxidation of β -Pinene, *Environ. Sci. Technol.*, 55, 15658–15671, <https://doi.org/10.1021/acs.est.1c03978>, 2021.
- Shen, H., Vereecken, L., Kang, S., Pullinen, I., Fuchs, H., Zhao, D., and Mentel, T. F.: Unexpected significance of a minor reaction pathway in daytime formation of biogenic highly oxygenated organic compounds, *Sci. Adv.*, 8, 1–11, 2022.
- Taatjes, C. A.: Uncovering the Fundamental Chemistry of Alkyl + O_2 Reactions via Measurements of Product Formation, *J. Phys. Chem. A*, 110, 4299–4312, 2006.
- Tomaz, S., Wang, D., Zabalegui, N., Li, D., Lamkaddam, H., Bachmeier, F., Vogel, A., Monge, M. E., Perrier, S., Baltensperger, U., George, C., Rissanen, M., Ehn, M., El Haddad, I., and Riva, M.: Structures and reactivity of peroxy radicals and dimeric products revealed by online tandem mass spectrometry, *Nat. Commun.*, 12, 300, <https://doi.org/10.1038/s41467-020-20532-2>, 2021.
- Tröstl, J., Chuang, W. K., Gordon, H., Heinritzi, M., Yan, C., Molteni, U., Ahlm, L., Frege, C., Bianchi, F., Wagner, R., Simon, M., Lehtipalo, K., Williamson, C., Craven, J. S., Duplissy, J., Adamov, A., Almeida, J., Bernhammer, A. K., Breitenlechner, M., Brilke, S., Dias, A., Ehrhart, S., Flagan, R. C., Franchin, A., Fuchs, C., Guida, R., Gysel, M., Hansel, A., Hoyle, C. R., Jokinen, T., Junninen, H., Kangasluoma, J., Keskinen, H., Kim, J., Krapf, M., Kürten, A., Laaksonen, A., Lawler, M., Leiminger, M., Mathot, S., Möhler, O., Nieminen, T., Onnela, A., Petäjä, T., Piel, F. M., Miettinen, P., Rissanen, M. P., Rondo, L., Sarnela, N., Schobesberger, S., Sengupta, K., Sipilä, M., Smith, J. N., Steiner, G., Tomè, A., Virtanen, A., Wagner, A. C., Weingartner, E., Wimmer, D., Winkler, P. M., Ye, P., Carslaw, K. S., Curtius, J., Dommen, J., Kirkby, J., Kulmala, M., Riipinen, I., Worsnop, D. R., Donahue, N. M., and Baltensperger, U.: The role of low-volatility organic compounds in initial particle growth in the atmosphere, *Nature*, 533, 527–531, <https://doi.org/10.1038/nature18271>, 2016.
- Valiev, R. R., Hasan, G., Salo, V. T., Kubečka, J., and Kurten, T.: Intersystem Crossings Drive Atmospheric Gas-Phase Dimer Formation, *J. Phys. Chem. A*, 123, 6596–6604, <https://doi.org/10.1021/acs.jpca.9b02559>, 2019.
- Vereecken, L.: Replication Data for: Formation of highly oxygenated organic molecules from the oxidation of limonene by OH radical: significant contribution of H-abstraction pathway, Jülich DATA [data set], <https://doi.org/10.26165/JUELICH-DATA/9JVHEK>, 2023.
- Vereecken, L. and Nozière, B.: H migration in peroxy radicals under atmospheric conditions, *Atmos. Chem. Phys.*, 20, 7429–7458, <https://doi.org/10.5194/acp-20-7429-2020>, 2020.
- Vereecken, L. and Peeters, J.: Theoretical Study of the Formation of Acetone in the OH-Initiated Atmospheric Oxidation of α -Pinene, *J. Phys. Chem. A*, 104, 11140–11146, 2000.

- Vereecken, L. and Peeters, J.: The 1,5-H-shift in 1-butoxy: A case study in the rigorous implementation of transition state theory for a multitoramer system, *J. Chem. Phys.*, 119, 5159–5170, <https://doi.org/10.1063/1.1597479>, 2003.
- Vereecken, L. and Peeters, J.: Decomposition of substituted alkoxy radicals – part I: a generalized structure-activity relationship for reaction barrier heights, *Phys. Chem. Chem. Phys.*, 11, 9062–9074, <https://doi.org/10.1039/b909712k>, 2009.
- Vereecken, L. and Peeters, J.: A structure-activity relationship for the rate coefficient of H-migration in substituted alkoxy radicals, *Phys. Chem. Chem. Phys.*, 12, 12608–12620, <https://doi.org/10.1039/c0cp00387e>, 2010.
- Vereecken, L. and Peeters, J.: A theoretical study of the OH-initiated gas-phase oxidation mechanism of β -pinene ($C_{10}H_{16}$): first generation products, *Phys. Chem. Chem. Phys.*, 14, 3802–3815, <https://doi.org/10.1039/c2cp23711c>, 2012.
- Vereecken, L., Müller, J. F., and Peeters, J.: Low-volatility polyoxygenates in the OH-initiated atmospheric oxidation of α -pinene: impact of non-traditional peroxy radical chemistry, *Phys Chem Chem Phys*, 9, 5241–5248, [10.1039/b708023a](https://doi.org/10.1039/b708023a), 2007.
- Vereecken, L., Vu, G., Wahner, A., Kiendler-Scharr, A., and Nguyen, H. M. T.: A structure activity relationship for ring closure reactions in unsaturated alkylperoxy radicals, *Phys. Chem. Chem. Phys.*, 23, 16564–16576, <https://doi.org/10.1039/d1cp02758a>, 2021.
- Waring, M. S.: Secondary organic aerosol formation by limonene ozonolysis: Parameterizing multi-generational chemistry in ozone- and residence time-limited indoor environments, *Atmos. Environ.*, 144, 79–86, <https://doi.org/10.1016/j.atmosenv.2016.08.051>, 2016.
- Wei, D., Fuentes, J. D., Gerken, T., Trowbridge, A. M., Stoy, P. C., and Chamecki, M.: Influences of nitrogen oxides and isoprene on ozone-temperature relationships in the Amazon rain forest, *Atmos. Environ.*, 206, 280–292, <https://doi.org/10.1016/j.atmosenv.2019.02.044>, 2019.
- Whalley, L. K., Edwards, P. M., Furneaux, K. L., Goddard, A., Ingham, T., Evans, M. J., Stone, D., Hopkins, J. R., Jones, C. E., Karunaharan, A., Lee, J. D., Lewis, A. C., Monks, P. S., Moller, S. J., and Heard, D. E.: Quantifying the magnitude of a missing hydroxyl radical source in a tropical rainforest, *Atmos. Chem. Phys.*, 11, 7223–7233, <https://doi.org/10.5194/acp-11-7223-2011>, 2011.
- Williams, P. J. H., Boustead, G. A., Heard, D. E., Seakins, P. W., Rickard, A. R., and Chechik, V.: New Approach to the Detection of Short-Lived Radical Intermediates, *J. Am. Chem. Soc.*, 144, 15969–15976, <https://doi.org/10.1021/jacs.2c03618>, 2022.
- Xu, L., Møller, K. H., Crouse, J. D., Otkjær, R. V., Kjaergaard, H. G., and Wennberg, P. O.: Unimolecular Reactions of Peroxy Radicals Formed in the Oxidation of α -Pinene and β -Pinene by Hydroxyl Radicals, *J. Phys. Chem. A*, 123, 1661–1674, <https://doi.org/10.1021/acs.jpca.8b11726>, 2019.
- Xu, R., Thornton, J. A., Lee, B. H., Zhang, Y., Jaeglé, L., Lopez-Hilfiker, F. D., Rantala, P., and Petäjä, T.: Global simulations of monoterpene-derived peroxy radical fates and the distributions of highly oxygenated organic molecules (HOMs) and accretion products, *Atmos. Chem. Phys.*, 22, 5477–5494, <https://doi.org/10.5194/acp-22-5477-2022>, 2022.
- Yan, C., Nie, W., Äijälä, M., Rissanen, M. P., Canagaratna, M. R., Massoli, P., Junninen, H., Jokinen, T., Sarnela, N., Häme, S. A. K., Schobesberger, S., Canonaco, F., Yao, L., Prévôt, A. S. H., Petäjä, T., Kulmala, M., Sipilä, M., Worsnop, D. R., and Ehn, M.: Source characterization of highly oxidized multifunctional compounds in a boreal forest environment using positive matrix factorization, *Atmos. Chem. Phys.*, 16, 12715–12731, <https://doi.org/10.5194/acp-16-12715-2016>, 2016.
- Yan, C., Nie, W., Vogel, A. L., Dada, L., Lehtipalo, K., Stolzenburg, D., Wagner, R., Rissanen, M. P., Xiao, M., Ahonen, L., Fischer, L., Rose, C., Bianchi, F., Gordon, H., Simon, M., Heinritzi, M., Garmash, O., Roldin, P., Dias, A., Ye, P., Hofbauer, V., Amorim, A., Bauer, P. S., Bergen, A., Bernhammer, A. K., Breitenlechner, M., Brilke, S., Buchholz, A., Mazon, S. B., Canagaratna, M. R., Chen, X., Ding, A., Dommen, J., Draper, D. C., Duplissy, J., Frege, C., Heyn, C., Guida, R., Hakala, J., Heikkinen, L., Hoyle, C. R., Jokinen, T., Kangasluoma, J., Kirkby, J., Kontkanen, J., Kurten, A., Lawler, M. J., Mai, H., Mathot, S., Mauldin, R. L., Molteni, U., Nichman, L., Nieminen, T., Nowak, J., Ojdanic, A., Onnela, A., Pajunoja, A., Petaja, T., Piel, F., Quelever, L. L. J., Sarnela, N., Schallhart, S., Sengupta, K., Sipilä, M., Tome, A., Trostl, J., Vaisanen, O., Wagner, A. C., Ylisirnio, A., Zha, Q., Baltensperger, U., Carslaw, K. S., Curtius, J., Flagan, R. C., Hansel, A., Riipinen, I., Smith, J. N., Virtanen, A., Winkler, P. M., Donahue, N. M., Kerminen, V. M., Kulmala, M., Ehn, M., and Worsnop, D. R.: Size-dependent influence of NO_x on the growth rates of organic aerosol particles, *Sci. Adv.*, 6, eaay4945, <https://doi.org/10.1126/sciadv.aay4945>, 2020.
- Yu, J., Cocker, D. R., Griffin, R. J., Flagan, R. C., and Seinfeld, J. H.: Gas-phase ozone oxidation of monoterpenes: Gaseous and particulate products, *J. Atmos. Chem.*, 34, 207–258, <https://doi.org/10.1023/A:1006254930583>, 1999.
- Zhang, H., Yee, L. D., Lee, B. H., Curtis, M. P., Worton, D. R., Isaacman-VanWertz, G., Offenberg, J. H., Lewandowski, M., Kleindienst, T. E., Beaver, M. R., Holder, A. L., Lonnen, W. A., Docherty, K. S., Jaoui, M., Pye, H. O. T., Hu, W., Day, D. A., Campuzano-Jost, P., Jimenez, J. L., Guo, H., Weber, R. J., de Gouw, J., Koss, A. R., Edgerton, E. S., Brune, W., Mohr, C., Lopez-Hilfiker, F. D., Lutz, A., Kreisberg, N. M., Spielman, S. R., Hering, S. V., Wilson, K. R., Thornton, J. A., and Goldstein, A. H.: Monoterpenes are the largest source of summertime organic aerosol in the southeastern United States, *P. Natl. Acad. Sci. USA*, 115, 2038–2043, <https://doi.org/10.1073/pnas.1717513115>, 2018.
- Zhao, B., Shrivastava, M., Donahue, N. M., Gordon, H., Schervish, M., Shilling, J. E., Zaveri, R. A., Wang, J., Andreae, M. O., Zhao, C., Gaudet, B., Liu, Y., Fan, J., and Fast, J. D.: High concentration of ultrafine particles in the Amazon free troposphere produced by organic new particle formation, *P. Natl. Acad. Sci. USA*, 117, 25344–25351, <https://doi.org/10.1073/pnas.2006716117>, 2020.
- Zhao, D., Schmitt, S. H., Wang, M., Acir, I.-H., Tillmann, R., Tan, Z., Novelli, A., Fuchs, H., Pullinen, I., Wegener, R., Rohrer, F., Wildt, J., Kiendler-Scharr, A., Wahner, A., and Mentel, T. F.: Effects of NO_x and SO_2 on the secondary organic aerosol formation from photooxidation of α -pinene and limonene, *Atmos. Chem. Phys.*, 18, 1611–1628, <https://doi.org/10.5194/acp-18-1611-2018>, 2018.
- Zhao, D., Pullinen, I., Fuchs, H., Schrade, S., Wu, R., Acir, I.-H., Tillmann, R., Rohrer, F., Wildt, J., Guo, Y., Kiendler-Scharr, A., Wahner, A., Kang, S., Vereecken, L., and Mentel, T. F.: Highly

- oxygenated organic molecule (HOM) formation in the isoprene oxidation by NO_3 radical, *Atmos. Chem. Phys.*, 21, 9681–9704, <https://doi.org/10.5194/acp-21-9681-2021>, 2021.
- Zhao, D. F., Buchholz, A., Kortner, B., Schlag, P., Rubach, F., Kiendler-Scharr, A., Tillmann, R., Wahner, A., Flores, J. M., Rudich, Y., Watne, Å. K., Hallquist, M., Wildt, J., and Mentel, T. F.: Size-dependent hygroscopicity parameter (κ) and chemical composition of secondary organic cloud condensation nuclei, *Geophys. Res. Lett.*, 42, 10920–10928, <https://doi.org/10.1002/2015gl066497>, 2015a.
- Zhao, D. F., Kaminski, M., Schlag, P., Fuchs, H., Acir, I. H., Bohn, B., Häsel, R., Kiendler-Scharr, A., Rohrer, F., Tillmann, R., Wang, M. J., Wegener, R., Wildt, J., Wahner, A., and Mentel, T. F.: Secondary organic aerosol formation from hydroxyl radical oxidation and ozonolysis of monoterpenes, *Atmos. Chem. Phys.*, 15, 991–1012, <https://doi.org/10.5194/acp-15-991-2015>, 2015b.
- Zhao, Y. and Truhlar, D. G.: The M06 suite of density functionals for main group thermochemistry, thermochemical kinetics, non-covalent interactions, excited states, and transition elements: two new functionals and systematic testing of four M06-class functionals and 12 other functionals, *Theor. Chem. Account.*, 120, 215–241, <https://doi.org/10.1007/s00214-007-0310-x>, 2008.
- Zhao, Y., Thornton, J. A., and Pye, H. O. T.: Quantitative constraints on autoxidation and dimer formation from direct probing of monoterpene-derived peroxy radical chemistry, *P. Natl. Acad. Sci. USA*, 115, 12142–12147, <https://doi.org/10.1073/pnas.1812147115>, 2018.
- Ziemann, P. J. and Atkinson, R.: Kinetics, products, and mechanisms of secondary organic aerosol formation, *Chem. Soc. Rev.*, 41, 6582–6605, <https://doi.org/10.1039/c2cs35122f>, 2012.